Opposing roles for SNAP23 in secretion in exocrine and endocrine pancreatic cells

Masataka Kunii,[1,2] Mica Ohara-Imaizumi,[3] Noriko Takahashi,[4] Masaki Kobayashi,[5] Ryosuke Kawakami,[6] Yasumitsu Kondoh,[7] Takeshi Shimizu,[7] Siro Simizu,[8] Bangzhong Lin,[9] Kazuto Nunomura,[9] Kyota Aoyagi,[3] Mitsuyo Ohno,[4] Masaki Ohmuraya,[10] Takashi Sato,[1] Shin-ichiro Yoshimura,[2] Ken Sato,[1] Reiko Harada,[2,11] Yoon-Jeong Kim,[9] Hiroyuki Osada,[7] Tomomi Nemoto,[6] Haruo Kasai,[4] Tadahiro Kitamura,[5] Shinya Nagamatsu,[3] and Akihiro Harada[1,2]

[1]Laboratory of Molecular Traffic, Department of Molecular and Cellular Biology, Institute for Molecular and Cellular Regulation, Gunma University, Gunma 371-8512, Japan
[2]Department of Cell Biology, Graduate School of Medicine, Osaka University, Osaka 565-0871, Japan
[3]Department of Biochemistry, Kyorin University School of Medicine, Tokyo 181-8611, Japan
[4]Laboratory of Structural Physiology, Graduate School of Medicine, Center for Disease Biology and Integrative Medicine, The University of Tokyo, Tokyo 113-0033, Japan
[5]Metabolic Signal Research Center, Institute for Molecular and Cellular Regulation, Gunma University, Gunma 371-8512, Japan
[6]Laboratory of Molecular and Cellular Biophysics, Research Institute for Electronic Science, Hokkaido University, Hokkaido 001-0020, Japan
[7]Chemical Biology Research Group, RIKEN Center for Sustainable Resource Science, Saitama 351-0198, Japan
[8]Department of Applied Chemistry, Faculty of Science and Technology, Keio University, Kanagawa 223-8522, Japan
[9]Drug Discovery Team, Office for University-Industry Collaboration Planning and Promotion, Osaka University, Osaka 565-0871, Japan
[10]Institute of Resource Development and Analysis, Kumamoto University, Kumamoto 860-0811, Japan
[11]Department of Judo Therapy, Takarazuka University of Medical and Health Care, Hyogo 666-0152, Japan

The membrane fusion of secretory granules with plasma membranes is crucial for the exocytosis of hormones and enzymes. Secretion disorders can cause various diseases such as diabetes or pancreatitis. Synaptosomal-associated protein 23 (SNAP23), a soluble *N*-ethyl-maleimide sensitive fusion protein attachment protein receptor (SNARE) molecule, is essential for secretory granule fusion in several cell lines. However, the in vivo functions of SNAP23 in endocrine and exocrine tissues remain unclear. In this study, we show opposing roles for SNAP23 in secretion in pancreatic exocrine and endocrine cells. The loss of SNAP23 in the exocrine and endocrine pancreas resulted in decreased and increased fusion of granules to the plasma membrane after stimulation, respectively. Furthermore, we identified a low molecular weight compound, MF286, that binds specifically to SNAP23 and promotes insulin secretion in mice. Our results demonstrate opposing roles for SNAP23 in the secretion mechanisms of the endocrine and exocrine pancreas and reveal that the SNAP23-binding compound MF286 may be a promising drug for diabetes treatment.

Introduction

Newly synthesized secretory proteins, such as hormones and digestive enzymes, are secreted through the fusion of secretory vesicles with the plasma membrane, which is mediated by SNA RE proteins (Hong, 2005; Jahn and Scheller, 2006; Südhof and Rothman, 2009; Thorn and Gaisano, 2012; Hong and Lev, 2014). One v-SNARE protein, namely vesicle-associated membrane protein (VAMP), and two t-SNARE proteins, namely syntaxin and SNAP, form an α-helical ternary complex to initiate membrane fusion. Regulation of exocytosis by SNAREs is essential for the secretion of neurotransmitters, hormones, enzymes, and cytokines from various tissues and cells.

In humans, 38 SNARE proteins have been identified (Hong and Lev, 2014). Each SNARE protein exhibits distinct tissue expression and intracellular localization as well as complex formation with its appropriate partners. For example, the VAMP2–syntaxin1A–SNAP25 complex, which is the best-characterized neuronal SNARE complex, catalyzes synaptic vesicle fusion at the presynaptic terminal (Sutton et al., 1998). This complex also promotes the fusion of insulin granules in pancreatic β cells (Hou et al., 2009; Kasai et al., 2012).

SNAP23 is a ubiquitously expressed homologue of SNAP25 (Ravichandran et al., 1996; Wang et al., 1997). Although SNAP25 plays critical roles in neurotransmitter release

Correspondence to Akihiro Harada: aharada@acb.med.osaka-u.ac.jp

Abbreviations used: AcKO, acinar cell (exocrine)–specific knockout; BcKO, β cell (endocrine)–specific knockout; CCK, cholecystokinin; HDL, high-density lipoprotein; HE, hematoxylin and eosin; hGH, human growth hormone; IPG TT, i.p. glucose tolerance test; IPR, isoproterenol; ITT, insulin tolerance test; KRB, Krebs-Ringer buffer; MeCh, methacholine; PcKO, pancreatic and duodenal homeobox gene 1–Cre-derived conditional knockout; RIP, rat insulin promoter II; SPR, surface plasmon resonance; SRB, sulforhodamine B; TEM, transmission electron microscopy; TIRFM, total internal reflection fluorescence microscopy; VAMP, vesicle-associated membrane protein; ZG, zymogen granule.

The Rockefeller University Press $30.00
J. Cell Biol. Vol. 215 No. 1 121–138
www.jcb.org/cgi/doi/10.1083/jcb.201604030

from neurons and insulin secretion from pancreatic β cells (Washbourne et al., 2002; Takahashi et al., 2010), SNAP23 is involved in exocytotic events in diverse nonneuronal cells, such as surfactant release from alveolar epithelial cells, glucose transporter GLUT4 translocation in adipocytes, and Ig release from plasma cells (Kawanishi et al., 2000; Abonyo et al., 2004; Reales et al., 2005). In pancreatic β cells, SNAP23 also promotes the fusion of insulin granules to the plasma membrane (Sadoul et al., 1997), whereas in pancreatic acinar cells, SNAP23 binds VAMP2 or VAMP8 for the fusion of amylase granules to the plasma membrane (Wang et al., 2004; Weng et al., 2007; Cosen-Binker et al., 2008). Thus, in vitro studies have suggested that SNAP23 is physiologically essential. However, the in vivo function of SNAP23 in the fusion of secretory granules remains largely unknown.

In this study, we generated pancreatic exocrine- or endocrine-specific *Snap23* knockout (KO) mice to investigate the in vivo function of SNAP23. The exocrine-specific KO mice showed decreased fusion of zymogen granules (ZGs), but the endocrine-specific KO mice showed increased fusion of insulin granules and improved glucose tolerance. These results suggest that SNAP23 plays opposite roles in secretion in the exocrine and endocrine pancreas. Furthermore, we found that the SNAP23-binding compound MF286 promoted insulin secretion and improved glucose tolerance by inhibiting formation of the SNARE complex that includes SNAP23. As MF286 also inhibits amylase secretion from the exocrine pancreas, as seen in exocrine-specific *Snap23* KO mice, our study indicated that MF286 might be a candidate drug for diabetes and pancreatitis treatment.

Results

Mouse models for pancreatic exocrine-specific and endocrine-specific SNAP23 KO mice

To determine the in vivo function of SNAP23, we generated *Snap23* conditional KO mice using a revertible KO system (Sato et al., 2007; Fig. 1 A). Consistent with a previous study (Suh et al., 2011), the homozygous mutant mice ($Snap23^{-/-}$ and $Snap23^{geo/geo}$) exhibited embryonic lethality before 8.5 d postcoitum (Fig. 1 B).

In the mouse and human pancreas, SNAP23 was expressed in both the pancreatic islets (endocrine) and acini (exocrine), but SNAP25 was expressed only in the islets (Fig. 1, C and D). Because these data suggest that SNAP23 participates in both the secretion of insulin from β cells and the secretion of digestive enzymes from acinar cells, we generated acinar cell (exocrine)–specific KO (AcKO) mice and β cell (endocrine)–specific KO (BcKO) mice. The AcKO mice (Elastase-Cre; $Snap23^{floxed/-}$ or $^{floxed/floxed}$) were generated by crossing *Snap23* floxed mice ($Snap23^{floxed/floxed}$) with Elastase-Cre mice (Hashimoto et al., 2008) expressing Cre recombinase by the elastase promoter. BcKO mice (rat insulin promoter II [RIP]–Cre; $Snap23^{floxed/-}$ or $^{floxed/floxed}$) were generated by crossing $Snap23^{floxed/floxed}$ with RIP-Cre mice expressing Cre recombinase by RIP (Herrera, 2000; Kitamura et al., 2009). Pancreatic and duodenal homeobox gene [Pdx] 1–Cre-derived conditional KO (PcKO; Pdx1-Cre; $Snap23^{floxed/-}$ or $^{floxed/floxed}$) mice were generated by crossing with Pdx1-Cre mice expressing Cre recombinase by the Pdx1 promoter (Gu et al., 2002). AcKO, BcKO, and PcKO mice were born at the expected Mendelian frequency and appeared overtly normal.

SNAP23 is essential for ZG exocytosis in pancreatic acinar cells

The AcKO mice, namely the pancreatic acinar cell (exocrine)–specific SNAP23 KO mice, appeared healthy. The body weights and serum biochemical figures were similar between control and AcKO mice (Fig. 2 A and Table 1). Immunofluorescence and Western blot analysis showed that SNAP23 levels on the plasma membrane were greatly decreased in acinar cells (Fig. 2, B and C).

The v-SNARE proteins VAMP2 and VAMP8 are crucial for the exocytosis of ZGs in the acinar cells, and SNAP23 is suggested to be a binding partner of VAMP2 or VAMP8 (Wang et al., 2004; Weng et al., 2007; Cosen-Binker et al., 2008). Therefore, we hypothesized that SNAP23 is involved in ZG exocytosis. To test this, we analyzed the density of ZGs in the acinar cells by light and electron microscopy. First, we observed the morphology and size of acinar cells by hematoxylin and eosin (HE) staining, but we could find no difference between control and AcKO acinar cells (Fig. 2 D). We next used transmission electron microscopy (TEM), but, again, the ZG density in AcKO cells was not significantly different. However, after cholecystokinin (CCK) stimulation, which evokes secretion of digestive enzymes by fusion of the ZGs with the apical membrane, the ZG density in AcKO cells was significantly higher (Fig. 2, E and F). This result suggested that ZG exocytosis was reduced in AcKO acinar cells.

To determine whether the secretion of digestive enzyme was reduced in AcKO acinar cells, we performed an in vitro amylase secretion assay using a colorimetric assay. Consistent with the result from the TEM analysis, we confirmed the reduction of amylase secretion in AcKO cells after CCK stimulation (Fig. 2 G). Furthermore, to check the effects of altered lipase secretion, we examined the lipids in stools. In AcKO stools, Sudan III staining showed many lipid droplets (Fig. 2 H), and percentage of fecal triglyceride was significantly increased (Fig. 2 I). These results suggest that the decreased lipase secretion leads to the lipid indigestion in AcKO mice.

ZGs are secreted by compound exocytosis, which is caused by an increase in intracellular Ca^{2+} concentration. In this process, primary fusion events occur in which the first granules fuse with the cell membrane, and this is followed by sequential fusion events in which secondary granules fuse onto these primary granules (Nemoto et al., 2001; Pickett and Edwardson, 2006; Kasai et al., 2012; Thorn and Gaisano, 2012). To investigate the frequency of ZG fusion, we counted the number of exocytotic events and monitored intracellular Ca^{2+} signaling using two-photon microscopy (Nemoto et al., 2001). Isolated acinar cells were immersed in a solution containing sulforhodamine B (SRB) as a fluid-phase tracer, and the primary and sequential exocytotic events were detected as the abrupt appearance of small fluorescent spots (Fig. 3 and Video 1). In the AcKO cells, both the primary and sequential exocytotic fusion events were significantly reduced (Fig. 3, A–E). The ratio of sequential exocytotic events to primary exocytotic events was lower in the AcKO cells, suggesting that SNAP23 participates in both primary and sequential secretion (Fig. 3 F). In contrast to the difference in the exocytotic events, the intracellular Ca^{2+} oscillations and maximal increase during CCK stimulation were similar in the control and AcKO cells, excluding that the inhibition

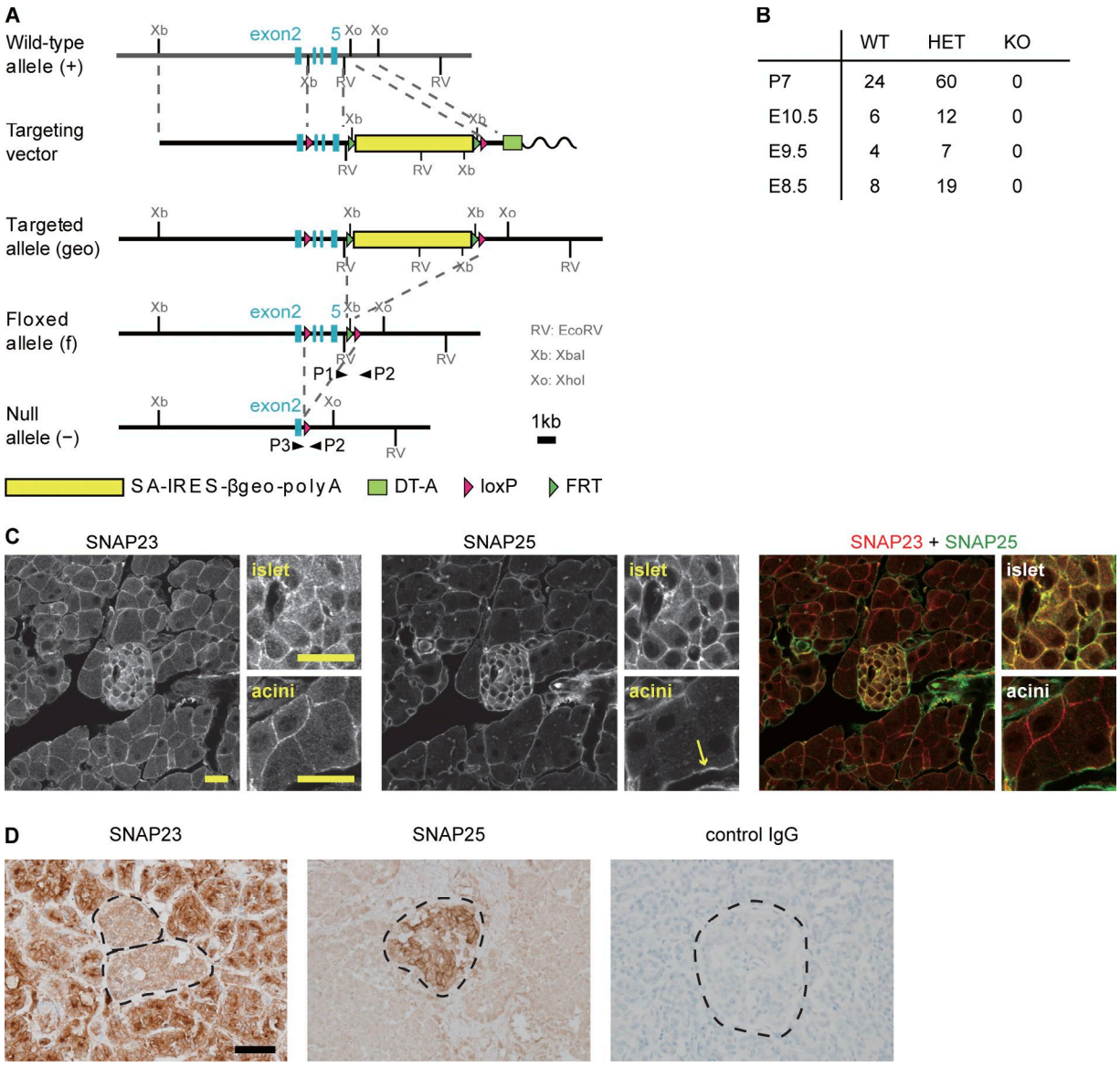

	WT	HET	KO
P7	24	60	0
E10.5	6	12	0
E9.5	4	7	0
E8.5	8	19	0

Figure 1. **Generation of *Snap23* KO mice and expression of SNAP23 and SNAP25 in the pancreas.** (A) Restriction maps of the wild-type allele, targeting vector, targeted allele, floxed allele, and null allele. Arrowheads indicate the position of the primers used for PCR screening. (B) Genotypic distribution of wild-type (WT; *Snap23*$^{+/+}$), heterozygous (HET; *Snap23*$^{+/-}$ and *Snap23*$^{+/geo}$), and KO (*Snap23*$^{-/-}$ and *Snap23*$^{geo/geo}$) mice at postnatal day (P) 7 and embryonic days (E) 10.5, 9.5, and 8.5, raised by intercrossing heterozygous pairs. No homozygous mutant SNAP23 mice (KO) were obtained. (C and D) In the wild-type pancreas, SNAP23 is localized in both the islets and acini, but SNAP25 is localized only in the islets. (C) Expression patterns of SNAP23 and SNAP25 in wild-type mouse pancreas shown by immunohistochemistry. High-magnification figures are shown in the top right (islet) and bottom right (acini). The SNAP25 antibody nonspecifically stained extracellular matrix surrounding lobules of acini (arrow). Bars, 20 µm. (D) Expression patterns of SNAP23 and SNAP25 in the human pancreas shown by immunohistochemistry. Regions surrounded by dashed lines indicate the pancreatic islets. Bar, 50 µm. IRES, internal ribosomal entry site; SA, splice acceptor.

of fusion events was a result of diminished Ca^{2+} concentration (Fig. 3, G and H). Collectively, we concluded that SNAP23 is essential for compound exocytosis in pancreatic acinar cells.

SNAP23 is also expressed in other exocrine tissues such as salivary glands (Wang et al., 2007). To confirm whether SNAP23 participates in the secretion in exocrine system in general, we measured the amylase secretion from parotid exocrine cells. Parotid exocrine cells were isolated from *Snap23* floxed mice (*Snap23*$^{floxed/floxed}$) and cultured with a Cre recombinase–encoding adenovirus (Ad-Cre) or with a control adenovirus (Ad-LacZ; Fig. 4 A). 48 h after infection, mRNA level of SNAP23 was greatly decreased (Fig. 4 B), and SNAP23 levels on the plasma membrane were decreased in Ad-Cre–treated cells (Fig. 4 C). Amylase secretion after isoproterenol (IPR) and methacholine (MeCh) stimulation was reduced in Ad-Cre–treated cells (Fig. 4 D). These results indicate that SNAP23 is also essential for secretion in other exocrine gland.

Loss of SNAP23 in the endocrine pancreas increases insulin secretion

The BcKO mice (RIP-Cre; *Snap23*$^{floxed/floxed}$ or $^{floxed/-}$) also grew normally, and serum biochemical tests showed no differences compared with the control mice (Fig. 5 A and Table 1). By immunofluorescence, SNAP23 localized to the plasma membrane in the control β cells but was absent in the BcKO β cells, confirming the successful depletion of SNAP23 in

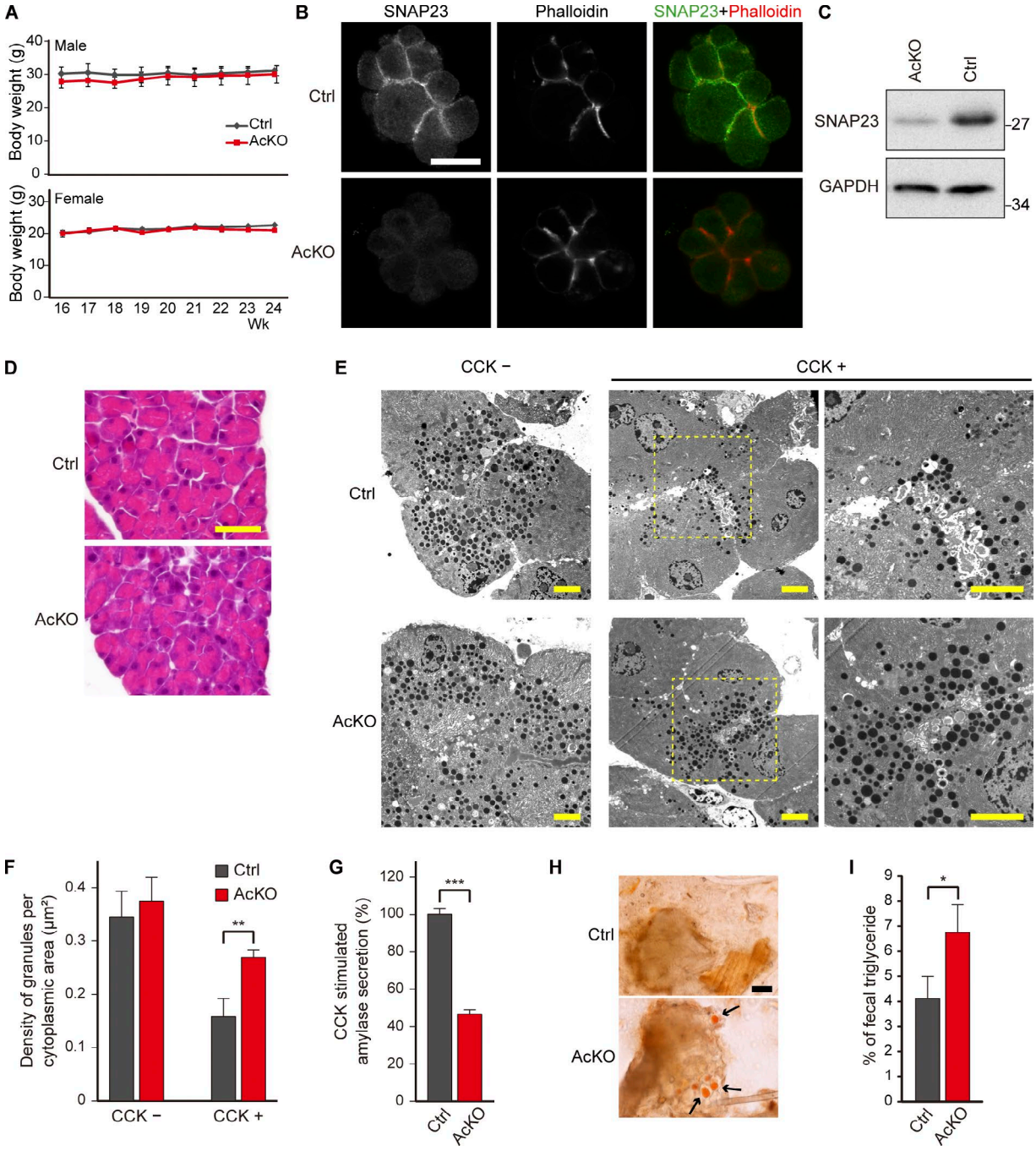

Figure 2. **Loss of SNAP23 results in decreased ZG secretion.** (A) Body weight of control (Ctrl) and AcKO mice. Three mice per genotype were examined. (B) SNAP23 and phalloidin (apical marker) staining in pancreatic acinar cells. SNAP23 localized to the plasma membrane in the control acinar cells, but the staining disappeared in the AcKO acinar cells. Bar, 20 µm. (C) SNAP23 levels evaluated by Western blotting in the islet-excluded pancreas tissue from control and AcKO mice. GAPDH was used as a loading control. A total of 20 µg protein is loaded in each well. (D) HE staining of the control and AcKO acinar cells. Bar, 50 µm. (E) Electron micrographs of acinar cells from control and AcKO mice without CCK stimulation (left panels) and after CCK stimulation (middle panel: low magnification; right panel: high magnification of the squares in the middle panel). Bars, 5 µm. (F) Quantification of ZG density per cytoplasmic area in ultrathin sections without CCK stimulation and after CCK stimulation. Analysis was performed on 8 control acinar cells and 10 AcKO acinar cells, scored in 2 mice per genotype. (G) Amylase secretion is reduced in AcKO acinar cells. Control and AcKO acinar cells were incubated with CCK, and the amount of secreted amylase was measured. The data are representative of three independent experiments. (H) Sudan III staining of stool smear preparation of control and AcKO mice. Arrows indicate lipid droplets. Bar, 50 µm. (I) Percentage of triglyceride in stools from control and AcKO mice. Three mice per genotype were used to collect stools. Data are mean ± SEM. Significance was calculated by the two-tailed paired Student's *t* test. *, $P < 0.05$; **, $P < 0.01$; ***, $P < 0.001$.

the BcKO β cells (Fig. 5 B). In contrast, the staining patterns and intensities of other SNARE proteins, such as SNAP25, syntaxin1A, and VAMP2, were similar between the control and BcKO islets (Fig. 5 B). The deletion of SNAP23 did not cause any overt change in the morphology of the islets, confirmed by HE staining (Fig. 5 C). We also found no differences in the expression levels of insulin, glucagon, and somatostatin (Figs. S1 and S2).

A previous study reported that SNAP23 promotes insulin secretion in HIT cells (Sadoul et al., 1997). Therefore, we speculated that glucose tolerance would be impaired in the BcKO mice. The blood glucose levels in the fasting or free-feeding mice were similar between the control and BcKO mice. Surprisingly, however, the blood glucose levels in the fasting-refeeding BcKO mice were significantly lower (Fig. 6 A). Furthermore, the serum insulin levels in the fasting-refeeding BcKO mice increased more than twofold (Fig. 6 B).

To further investigate the role of SNAP23 in glucose tolerance, we performed an i.p. glucose tolerance test (IPGTT). In agreement with the fasting-refeeding experiments, glycemia in response to glucose stimulation was significantly reduced in the BcKO mice (Fig. 6 C). The amount of secreted insulin 15 min after glucose injection was also dramatically increased (Fig. 6 D). In contrast, an insulin tolerance test (ITT) showed that the insulin sensitivity in the peripheral tissue was similar (Fig. 6 E), demonstrating that the decline in blood glucose levels during IPGTT was the result of increased insulin secretion of BcKO β cells.

To obtain precise information about the kinetics of insulin exocytosis, we isolated the islets and examined the insulin secretion (Fig. 6, F–H). When the islets were incubated with a low concentration (2.2 mM) of glucose, BcKO islets secreted similar levels of insulin as control islets. However, upon stimulation with a high concentration (16.7 mM) of glucose, BcKO islets secreted a significantly higher amount of insulin (Fig. 6 F).

There are at least two phases of the insulin secretion process: the initial rapid first phase and the sustained second phase (Hou et al., 2009). To check this secretion process, we performed a perfusion analysis in the isolated islets. The amount of secreted insulin was increased only during the first phase in the BcKO-perfused islets (Fig. 6, G and H). Additionally, we expressed insulin-GFP in β cells and observed the exocytotic events using total internal reflection fluorescence microscopy (TIRFM). The experiment revealed that the fusion events of the predocked granules but not the newcomer granules were increased in the BcKO islets (Fig. 6, I and J). These results suggest that SNAP23 inhibits the first phase of secretion by suppressing the fusion of predocked granules.

To confirm the phenotypes of BcKO mice, we generated additional SNAP23 PcKO mice (Gu et al., 2002). In the wild-type islets, SNAP23 was expressed in α and β cells but was scarcely expressed in δ cells, whereas SNAP25 was expressed in all three types of cells (Figs. S1 and S2). These data suggest that SNAP23 is involved in the secretion of insulin and glucagon. Because the Pdx1-Cre transgenic mice express the *cre* gene in all pancreatic cell types (Gu et al., 2002), we assumed that it recombined the *Snap23* floxed allele in both α and β cells in the islets. Unexpectedly, our PcKO mice showed that SNAP23 was depleted in most of the β cells but was present in the α cells (Fig. S1). This phenotype might be caused by a difference in genetic background. It is also reported that a difference in the target floxed allele affects the recombination efficiency in a given cell (Zheng et al., 2000; Heffner et al., 2012).

Similar to BcKO mice, an IPGTT experiment demonstrated that glucose tolerance was improved in the PcKO mice (Fig. S3 A). Furthermore, the serum insulin levels 30 min after glucose stimulation were increased in the PcKO mice (Fig. S3 B). To observe insulin exocytosis from the PcKO β cells, we counted the number of fusion events in the β cells using two-photon microscopy (Takahashi et al., 2002) (Fig. S3 C and Video 2). Consistent with the TIRFM analysis of BcKO islets, the fusion of insulin granules occurred more frequently during the initial 5 min in the PcKO islets (Fig. S3, D and E). The intracellular Ca^{2+} concentrations were similar between the control and PcKO islets (Fig. S3 F), excluding the possibility that the increased fusion events were a result of increased Ca^{2+} concentration.

By TEM, the β cell morphology and granule sizes were indistinguishable between the control and PcKO islets (Fig. S3, G and H). In addition, the numbers of total and docked insulin granules were similar (Fig. S3, I and J). These results suggest that the increased insulin secretion was not caused by abnormalities in the insulin granule.

Table 1. **Serum biochemistries among control, AcKO, and BcKO mice**

	Control	AcKO	BcKO
Age (wk)	19	19	20
n	*5*	*5*	*5*
Total protein (g/dl)	5.2 ± 0.07	5.0 ± 0.0	5.3 ± 0.13
Albumin (g/dl)	3.5 ± 0.1	3.7 ± 0.08	3.4 ± 0.09
Blood urea nitrogen (mg/dl)	26.8 ± 1.05	28.6 ± 1.06	25.1 ± 0.79
Creatinine (mg/dl)	0.1 ± 0.011	0.1 ± 0.009	0.1 ± 0.009
Na (mEq/l)	148.2 ± 0.66	147.2 ± 0.8	149.4 ± 0.68
K (mEq/l)	5.5 ± 0.13	5.4 ± 0.25	5.2 ± 0.15
Cl (mEq/l)	100.6 ± 2.1	98.0 ± 0.9	107.2 ± 3.4
Ca (mEq/l)	9.0 ± 0.09	9.2 ± 0.19	9.1 ± 0.08
Inorganic phosphorus (mg/dl)	6.8 ± 0.14	6.3 ± 0.1	6.1 ± 0.3
Aspartate aminotransferase (IU/l)	73.8 ± 5.2	66.4 ± 1.6	67.6 ± 3.1
Alanine aminotransferase (IU/l)	20.2 ± 1.7	18.8 ± 1.4	21.2 ± 2.0
Lactate dehydrogenase (IU/l)	300.0 ± 26.8	301.2 ± 25.4	231.0 ± 26.7
Amylase (IU/l)	3,371.2 ± 125.9	5,950.0 ± 963.6	4,213.6 ± 674.6
Total cholesterol (mg/dl)	82.8 ± 5.5	72.0 ± 4.9	79.4 ± 3.3
Triglycerides (mg/dl)	48.8 ± 11.6	38.8 ± 13.5	29.4 ± 3.4
HDL cholesterol (mg/dl)	45.8 ± 4.7	37.6 ± 3.0	46.6 ± 2.4
Total bilirubin (mg/dl)	0.1 ± 0.012	0.1 ± 0.005	0.1 ± 0.006
Glucose (mg/dl)	111.6 ± 7.7	112.4 ± 5.5	115.6 ± 5.9

Data are mean ± SEM unless otherwise noted.

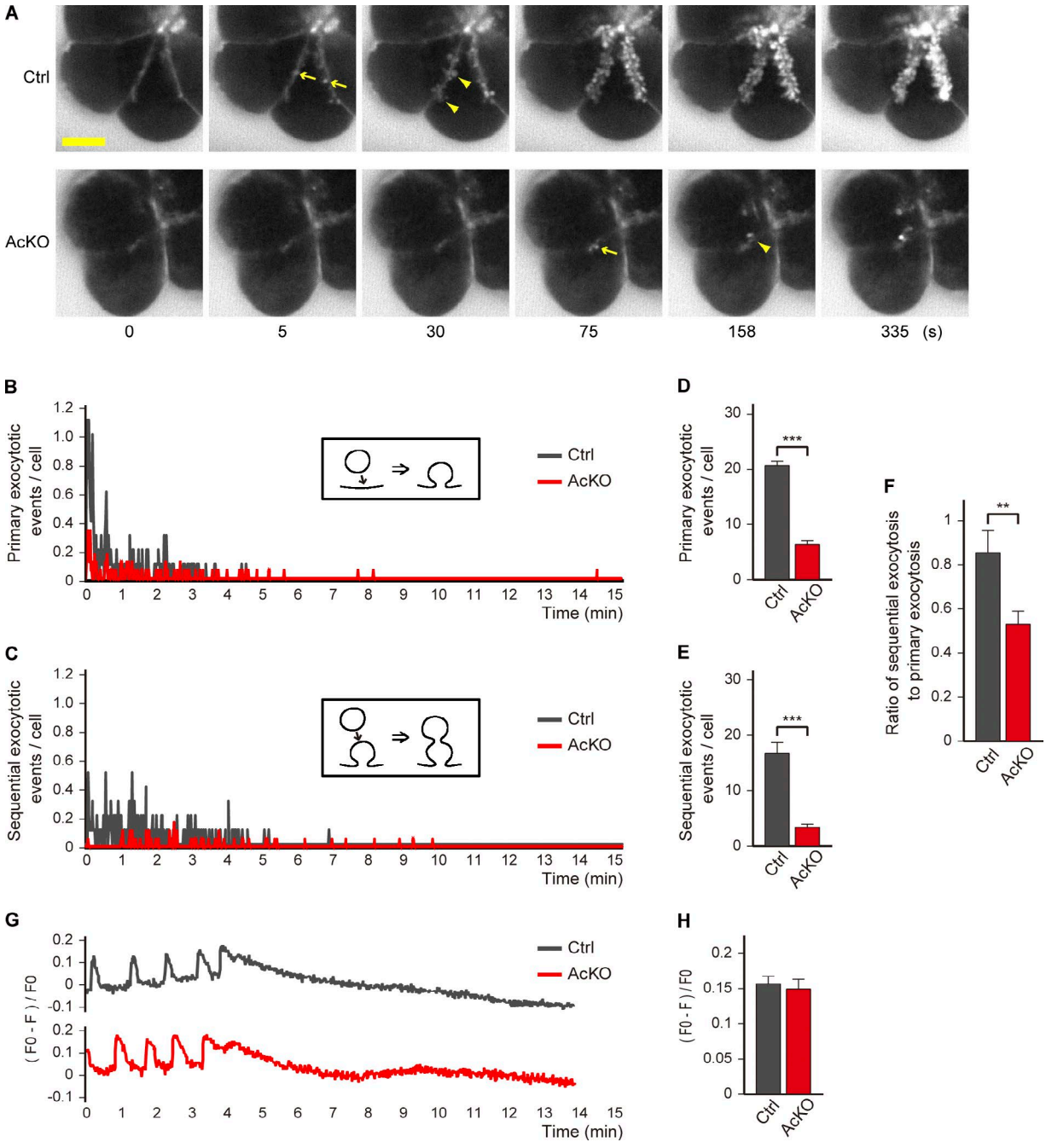

Figure 3. **Loss of SNAP23 reduces both the primary and sequential exocytosis fusion events in acinar cells.** (A) Fluorescence images of SRB during 100 pM CCK stimulation of control (Ctrl) and AcKO acinar cells. Arrows indicate primary exocytosis, and arrowheads indicate sequential exocytosis. Bar, 10 µm. (B–E) Quantification of exocytotic events in response to CCK stimulation. The numbers of primary (B) and sequential (C) exocytotic events detected by two-photon microscopy were counted in control and AcKO acinar cells. (D and E) show the total numbers of primary and sequential exocytosis per acinar cell during a 15-min period. 10 acinar cells from 4 control mice and 18 acinar cells from 6 AcKO mice were analyzed. (F) The ratio of sequential exocytotic events to primary exocytotic events calculated by the values of D and E. (G) Time courses of intracellular Ca^{2+} concentrations in the control (top) and AcKO (bottom) acinar cells during CCK stimulation as represented by $(F_0 - F)/F_0$, where F_0 and F are the resting and poststimulation fluorescence, respectively. (H) The maximum increment of intracellular Ca^{2+} concentrations. Nine acinar cells from two control mice and nine acinar cells from three AcKO mice were analyzed. Data are mean ± SEM. Significance was calculated by the two-tailed paired Student's *t* test. **, $P < 0.01$; ***, $P < 0.001$.

SNAP23 competes with SNAP25 for SNARE complex formation

Among the SNARE proteins, VAMP2, syntaxin1A, and SNAP25 are involved in the fusion between the insulin granules and the plasma membrane (Regazzi et al., 1995; Sadoul et al., 1995; Ohara-Imaizumi et al., 2007; Takahashi et al., 2015). The SNAP25–VAMP2–syntaxin1A complex is reported to exhibit tighter binding among its components and can fuse membranes more efficiently than the SNAP23–VAMP2–syntaxin1A complex during exocytosis (Sørensen et al., 2003; Vites et al., 2008; Montana et al., 2009). Therefore, we speculated that SNAP23 might compete with SNAP25 for binding to syntaxin1A and VAMP2. To test this, we performed in vitro binding competition studies using recombinant SNARE proteins. We incubated GST-

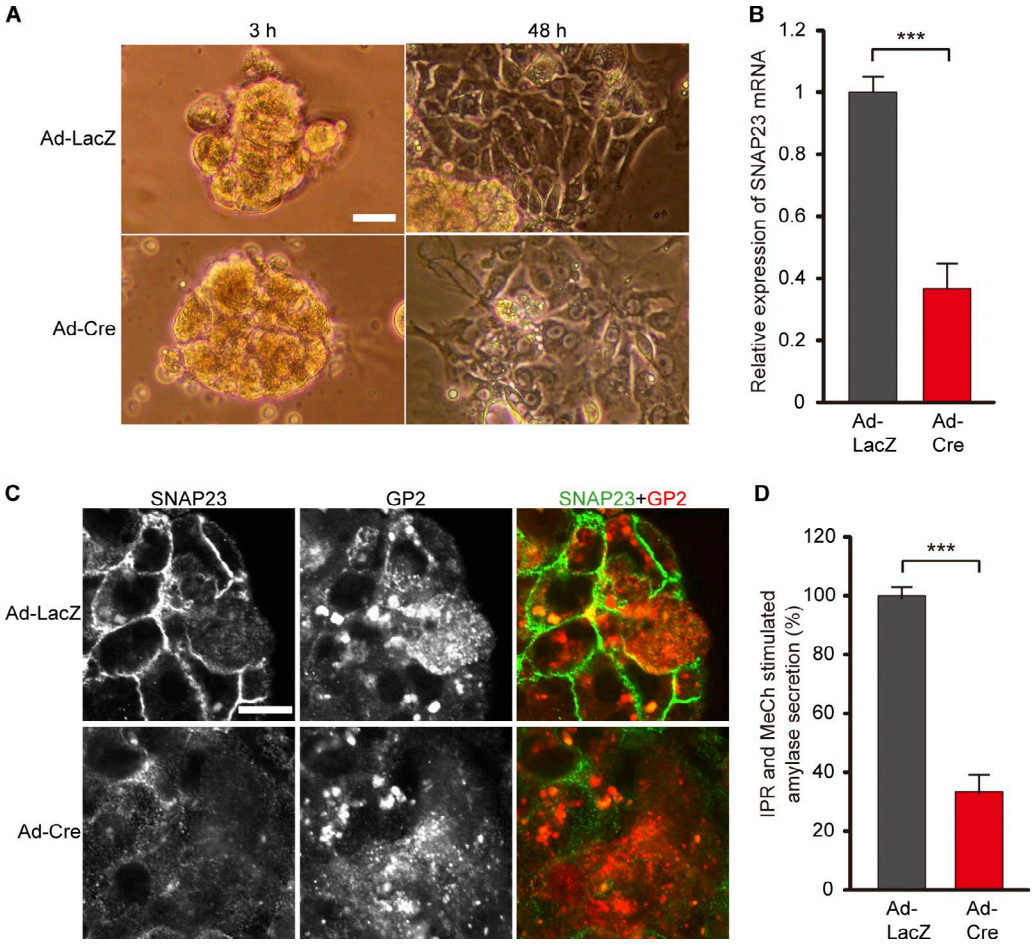

Figure 4. **Loss of SNAP23 results in decreased amylase secretion in parotid exocrine cells.** (A) Phase-contrast image of cultured parotid exocrine cells at 3 and 48 h after Ad-LacZ and Ad-Cre infection. Bar, 50 µm. (B) Relative expression levels of SNAP23 mRNA measured by real-time PCR at 48 h after adenovirus infection. Parotid exocrine cells from two mice were examined. (C) SNAP23 and GP2 (ZG marker) staining in parotid exocrine cells. SNAP23 localized to the plasma membrane in the Ad-LacZ–infected exocrine cells, but the staining disappeared in the Ad-Cre–infected exocrine cells. Bar, 10 µm. (D) Amylase secretion is reduced in Ad-Cre infected exocrine cells. Infected exocrine cells were incubated with IPR and MeCh, and the amount of secreted amylase was measured. Parotid exocrine cells from three mice were examined. Data are mean ± SEM. Significance was calculated by the two-tailed paired Student's *t* test. ***, $P < 0.001$.

SNAP25 with equal amounts of His-VAMP2 and His-syntaxin1A in the presence of variable concentrations of His-SNAP23. As shown in Fig. 7 A and illustrated in Fig. 7 B, increasing SNAP23 concentration inhibited the formation of the SNAP25–syntaxin1A–VAMP2 complex, confirming that SNAP23 competes with SNAP25 for binding to syntaxin1A and VAMP2.

SNAP23 forms a homotetrameric complex using its N-terminal coiled-coil domain (Freedman et al., 2003). Because the amino acid sequence of the coiled-coil region of SNAP23 is similar to the same region of SNAP25, SNAP23 might bind SNAP25 and disturb the formation of the SNAP25-containing SNARE complex, which participates in insulin granule fusion. To exclude this possibility, we performed an immunoprecipitation assay using islet lysates from wild-type mice. The levels of SNAP23 that coimmunoprecipitated with the antibody against SNAP25 and control IgG were equally low in the islet lysate (Fig. 7 C). This result suggests that SNAP23 does not bind SNAP25 in the pancreatic islets.

In the BcKO islets, we found no differences in the levels of SNAP25, syntaxin1A, and VAMP2. However, immunoprecipitation assays of control and BcKO islets revealed that the disruption of SNAP23 increased the amount of SNAP25-bound VAMP2 (Fig. 7, D and E). This indicates that SNAP23 depletion allowed the increased formation of SNAP25–VAMP2–syntaxin1A complexes, further resulting in the enhanced insulin secretion in the BcKO islets.

To verify this result using a simplified system, we used the mouse insulinoma-derived cell line MIN6 as a model β cell. We first addressed whether the knockdown of SNAP23 in MIN6 cells facilitated hormone secretion. MIN6 cells were transfected with human growth hormone (hGH) together with control siRNA, siRNA against SNAP23, or siRNA against SNAP25. As expected, the hormone secretion was significantly enhanced in SNAP23-knockdown MIN6 cells, whereas it was decreased in SNAP25-knockdown MIN6 cells compared with control cells (Fig. 7 F). We next performed an immunoprecipitation assay similar to Fig. 7 D using the SNAP23-knockdown MIN6 cells. Consistent with the result obtained by BcKO islets, the amount of VAMP2 in SNAP25 immunoprecipitates increased in SNAP23-knockdown MIN6 cells (Fig. 7, G and H). Collectively, our results suggest that the increased hormone exocytosis in the BcKO islets and SNAP23-knockdown MIN6 cells was caused by the increased formation of SNAP25–VAMP2–syntaxin1A complexes as a consequence of SNAP23 depletion.

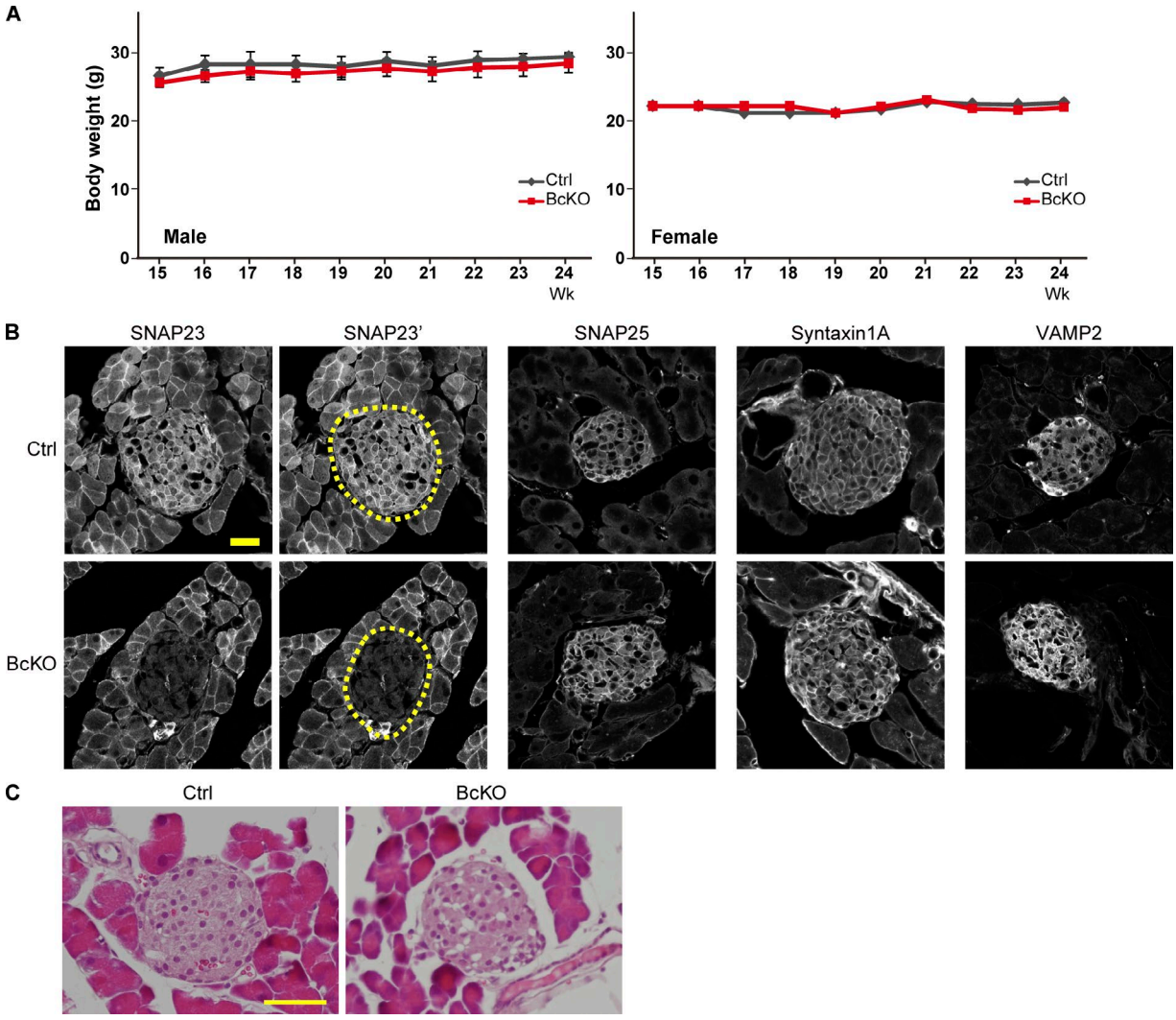

Figure 5. **Pancreatic β cell–specific disruption of SNAP23.** (A) Body weight of control (Ctrl) and BcKO mice. Three male mice and one female mouse per genotype were examined. (B) SNAP23, SNAP25, syntaxin1A, and VAMP2 staining in pancreatic islets. In SNAP23′, the dashed line indicates the outline of the islets. Bar, 50 µm. (C) HE staining of control and BcKO islets. Bar, 50 µm.

The SNAP23-binding compound MF286 promotes insulin secretion

Because SNAP23 depletion caused increased insulin secretion, we speculated that a SNAP23 inhibitor might be a new therapeutic drug candidate for diabetes. We screened a chemical compound library from RIKEN's NPDepo (Zimmermann et al., 2013) with GST-SNAP23 and GST-SNAP25 and identified five compounds that bound SNAP23 more strongly than SNAP25. For further screening, the amounts of insulin secretion were measured after treatment of MIN6 cells with each compound. As a result, we found that after treatment with compound 2, MF286, the amount of insulin was significantly increased in response to glucose stimulation (Fig. 8, A and B). The influence of these compounds on MIN6 cell survival was low, which excluded the possibility that general toxicity affected insulin secretion (Fig. 8 C). The kinetic curves of surface plasmon resonance (SPR) showed that MF286 definitely bound SNAP23, but it barely bound SNAP25, demonstrating that the specific inhibition of SNAP23 resulted in the enhanced insulin secretion (Fig. 8 D).

The addition of MF286, up to 0.01 µM, also increased insulin secretion in the isolated islets in a dose-dependent manner (Fig. 8 E). However, it was less effective at higher concentrations, presumably because of cytotoxicity against the primary β cells. These results indicate that a suitable dose of MF286 increased insulin secretion through SNAP23 inhibition.

To determine the effect of MF286 in vivo, we injected MF286 i.p. into wild-type mice and performed an IPGTT. The blood glucose levels in MF286-injected mice were significantly lower than in PBS-injected mice 30 min after glucose stimulation (Fig. 9 A). Furthermore, the serum insulin levels in the MF286-injected mice were higher than in the uninjected mice (Fig. 9 B). In contrast, ITT revealed similar insulin sensitivities in the mice independent of MF286 treatment (Fig. 9 C). These results suggested that MF286 effectively increased insulin secretion in vivo.

To understand the associated molecular mechanism, we analyzed the effect of MF286 on SNARE complex formation using in vitro GST-pulldown assays. When we added MF286 to a mixture that contained SNAP23, VAMP2, and syntaxin1A, the amount of VAMP2 that bound the syntaxin1A–SNAP23 complex was clearly reduced (Fig. 9 D, left). In contrast, when we added MF286 to a mixture of SNAP25, VAMP2, and syntaxin1A, the

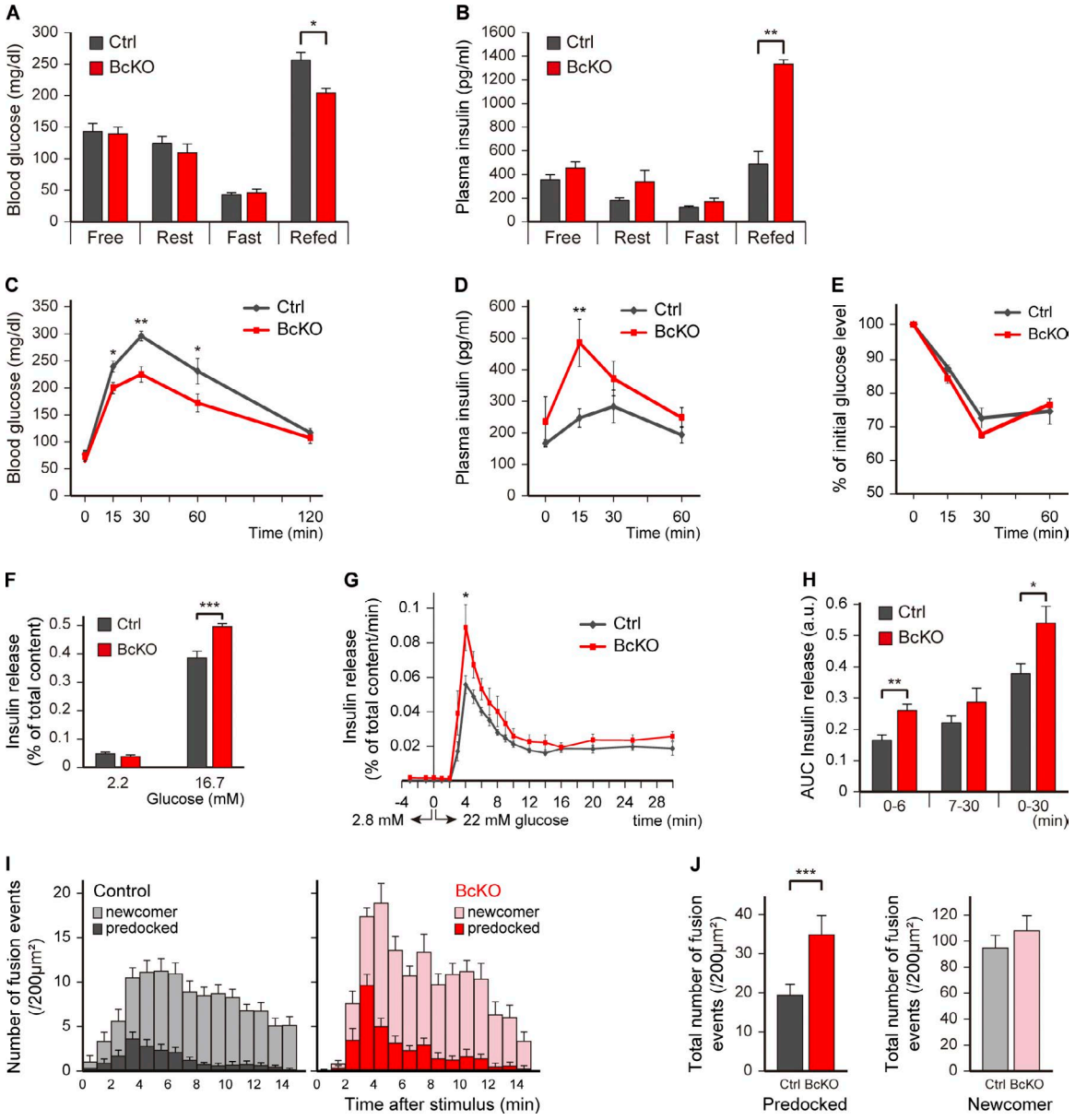

Figure 6. **SNAP23 deletion increases exocytosis of predocked granules during biphasic insulin release.** (A and B) Fasting-refeeding experiments showing the enhanced glucose tolerance in BcKO mice. Blood glucose concentrations (A) and plasma insulin concentrations (B) under conditions of feeding (Free), 2-h fasting (Rest), 18-h fasting (Fast), and refeeding after 18-h fasting (Refed). Four mice per genotype were examined for blood glucose concentrations, and three mice per genotype were examined for plasma insulin concentrations. Blood glucose concentrations (C) and plasma insulin concentrations (D) during IPGTT. Three mice per genotype were examined. (E) Percentage of initial blood glucose concentration during ITT. Three mice per genotype were examined. (F) Insulin secretion from isolated islets as measured by a batch assay. Islets were isolated from control (Ctrl) and BcKO mice by collagenase digestion, and, after a 30-min incubation with 2.2 mM or 16.7 mM glucose, the secreted insulin was measured by ELISA. The total contents of insulin were obtained by solubilizing and sonicating the islets after the experiments. Islets from three mice per genotype were examined. (G and H) Perfusion analysis of isolated islets demonstrating the increased insulin secretion of BcKO islets in the first phase (4 min after 22 mM glucose induction). Islets from three mice per genotype were examined. (I and J) TIRFM analysis showing that the predocked insulin granules fusion was increased in the BcKO islets. (I) Histogram of the number of fusion events in control and BcKO β cells at 1-min intervals after 22 mM glucose stimulation observed by TIRFM. (J) The total number of fusion events of predocked or newcomer granules calculated by the values of I. Analysis was performed on 28 control β cells and 20 BcKO β cells scored in six mice per genotype. Data are mean ± SEM. Significance was calculated by the two-tailed paired Student's *t* test. *, $P < 0.05$; **, $P < 0.01$; ***, $P < 0.001$. a.u., arbitrary units.

amount of VAMP2 that bound the syntaxin1A–SNAP25 complex remained unaltered (Fig. 9 D, right). These results suggest that MF286 specifically inhibits the formation of SNAP23–VAMP2–syntaxin1A complexes and that this inhibition may result in the increased formation of SNAP25–VAMP2–syntaxin1A complexes.

Next, to check whether the effect of MF286 is specific to SNAP23, we performed an IPGTT using BcKO mice. We assumed that if MF286 reduce blood glucose levels through any other different molecules from SNAP23, it would reduce blood glucose even in BcKO mice. However, the blood glucose levels in MF286-injected BcKO mice showed no significant differences compared with PBS-injected BcKO mice (Fig. S4 A). Plasma insulin levels after glucose stimulation also similar between these mice (Fig. S4 B). These results suggest that the

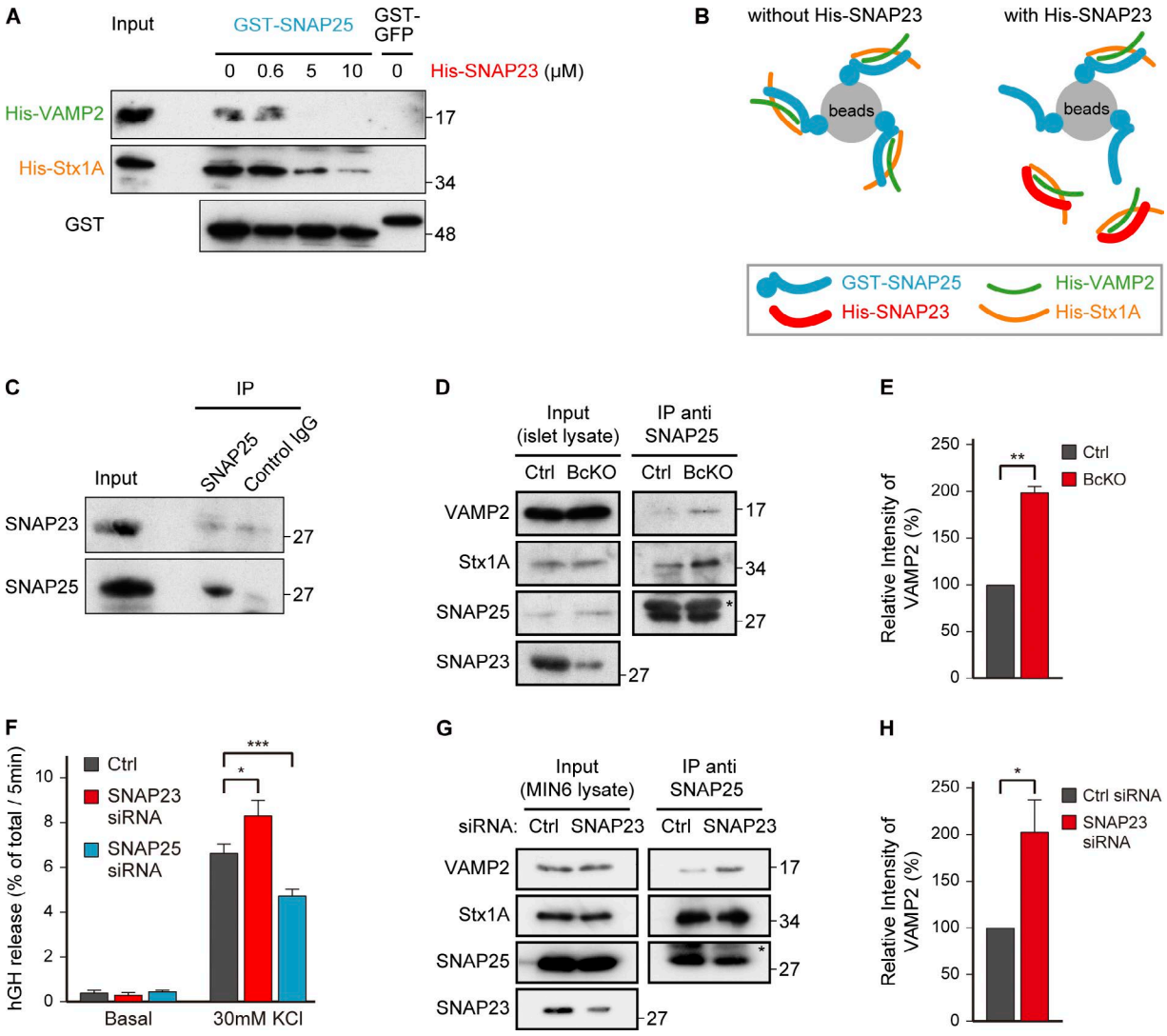

Figure 7. **Loss of SNAP23 results in increased amounts of the syntaxin1A (Stx1A)–VAMP2–SNAP25 complex.** (A) In vitro competition experiment demonstrating that SNAP23 and SNAP25 compete with each other for binding to Stx1A and VAMP2. His-SNAP23 (0, 0.6, 5, and 10 µM), His-Stx1A, and His-VAMP2 (0.6 µM each) were mixed to form recombinant SNARE complex and then combined with GST-SNAP25 (0.6 µM) and glutathione beads. The beads were analyzed by SDS-PAGE and immunoblotting. (B) Scheme of SNAP23 competing with SNAP25 for binding to Stx1A and VAMP2 in the GST pulldown assay. (C) SNAP23 did not coimmunoprecipitate with SNAP25. Islet lysates from wild-type mice were immunoprecipitated (IP) with antibodies against SNAP25 and control IgG. (D) Coimmunoprecipitation of Stx1A and VAMP2 in SNAP25 immunoprecipitates from control (Ctrl) and BcKO islet lysates. The asterisk indicates the IgG light chain. (E) VAMP2 intensity in the SNAP25 immunoprecipitates from BcKO relative to control islet lysates. The data are representative of three independent experiments. (F) KCl-induced secretion of hGH from MIN6 cells transfected with hGH together with control siRNA, siRNA against SNAP23, or siRNA against SNAP25, as measured by a batch release assay and an ELISA. The data are representative of five independent experiments. (G and H) Coimmunoprecipitation of Stx1A and VAMP2 in SNAP25 immunoprecipitates from control siRNA–treated or SNAP23 siRNA–treated MIN6 cell lysates. The asterisk indicates the IgG light chain. (H) VAMP2 intensity in the SNAP25 immunoprecipitates from SNAP23-knockdown MIN6 relative to control MIN6 cell lysates. The data are representative of three independent experiments. Data are mean ± SEM. Significance was calculated by the two-tailed paired Student's *t* test. *, $P < 0.05$; **, $P < 0.01$; ***, $P < 0.001$.

increased insulin secretion by MF286 injection is caused by the inhibitory effect of MF286 against only SNAP23.

In peripheral tissues such as the adipose tissue and muscle, glucose is incorporated into cells through the GLUT4 glucose transporter after insulin stimulation. SNAP23 participates in GLUT4 translocation through binding to VAMP2 and syntaxin4 (Kawanishi et al., 2000). To understand the effect of MF286 on the SNAP23, VAMP2, and syntaxin4 complex formation, we performed a GST-pulldown assay. We found no influence of MF286 on the SNARE complex formation among these SNARE proteins (Fig. 9 E). Furthermore, GLUT4 translocation and the uptake of 2-deoxyglucose were not altered in MF286-treated 3T3-L1 adipocytes after insulin stimulation (Fig. 9, F and G). These results suggest that MF286 does not affect GLUT4 translocation in the adipocytes. This is also supported from the previous in vivo ITT, in which glucose uptake was unchanged regardless of MF286 injection.

We also analyzed the effect of MF286 on secretion in the pancreatic acinar cells. The amount of secreted amylase in the MF286-treated acinar cells was significantly decreased (Fig. 9 H), indicating that MF286 inhibits the SNARE complex formation required for ZG fusion in the pancreatic acinar cells.

Finally, we examined whether long-term treatment of MF286 causes adverse effects. MF286 was injected i.p. into

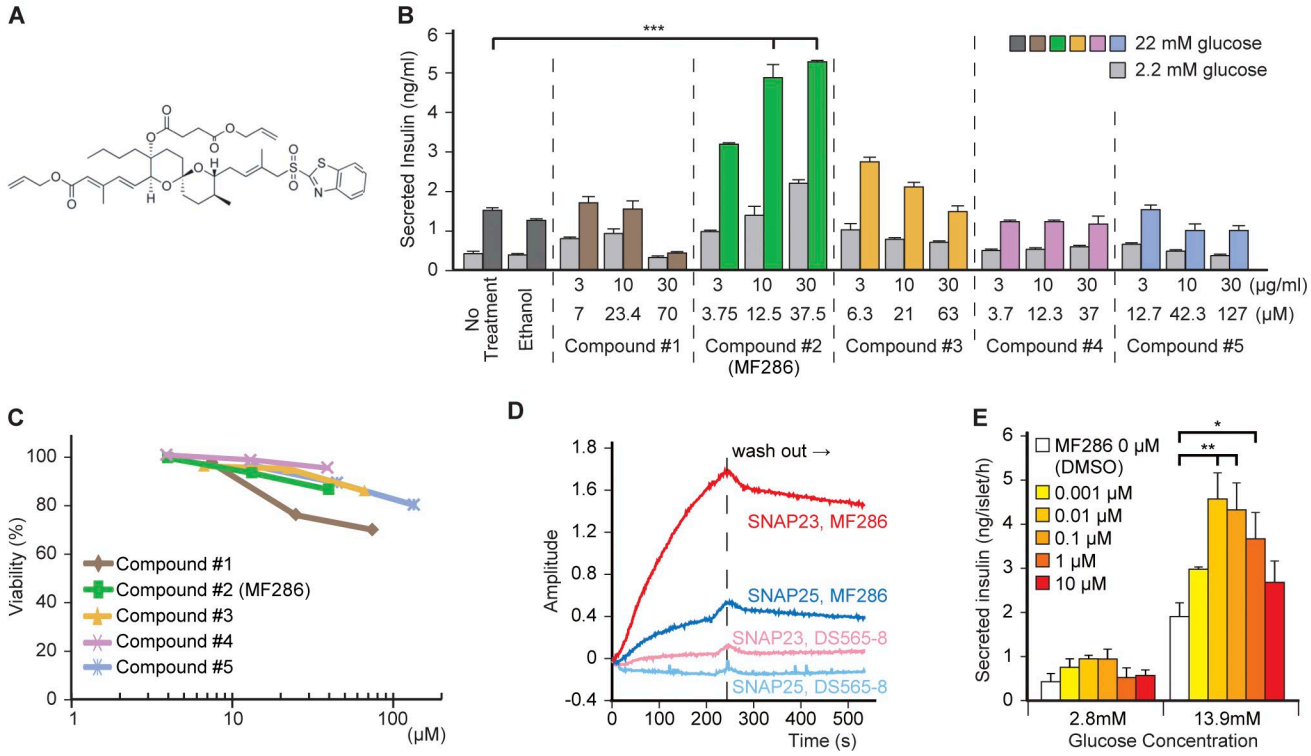

Figure 8. **MF286 increases insulin secretion in vivo.** (A) A structural diagram of MF286. (B) Secreted insulin concentrations from MIN6 cells after treatment with chemical compounds after low (2.2 mM) or high (22 mM) glucose stimulation. The molar concentrations of each compound, which correspond to experimental concentrations (3, 10, and 30 μg/ml), were indicated. The data are representative of three independent experiments. (C) Survival curves of MIN6 cells after treatment with chemical compounds. (D) SPR measuring MF286 or DS565-8 binding to SNAP23 or SNAP25. DS565-8 was used as a negative control. (E) Secreted insulin concentrations from isolated islets after MF286 treatments after low (2.8 mM) or high (13.9 mM) glucose stimulation. The data are representative of three independent experiments. Data are mean ± SEM. Significance was calculated by the two-tailed paired Student's *t* test. *, P < 0.05; **, P < 0.01; ***, P < 0.001.

wild-type mice once per day for 30 d. Serum biochemical tests showed no differences between PBS- and MF286-injected mice before or after repetitive injection (Fig. S5 A and Table 2). HE staining of various organs also showed no abnormality in MF286-injected mice (Fig. S5 B). These results suggest that MF286 does not cause the adverse effects at least 30 d after injection and may be a safer drug candidate for diabetes.

Discussion

SNAP23 is essential for exocytosis in various nonneuronal tissues, including the exocrine and endocrine pancreas (Sadoul et al., 1997; Kawanishi et al., 2000; Abonyo et al., 2004; Reales et al., 2005). However, as the function of SNAP23 in regulated secretion in vivo remained unclear, we generated and analyzed both exocrine and endocrine pancreas-specific KO mice.

In the exocrine pancreas, previous studies suggested that in vitro, SNAP23 bound syntaxin2/VAMP2 for primary (ZG-to-plasma membrane) fusion or syntaxin3/VAMP8 for sequential (ZG-to-ZG) fusion (Wang et al., 2004; Weng et al., 2007; Behrendorff et al., 2011). In this study, our results provide direct evidence that SNAP23 promotes both types of fusion in the exocrine pancreas also in vivo. Furthermore, amylase secretion was also decreased in SNAP23 KO parotid exocrine cells, suggesting that SNAP23 is essential for exocytosis in the exocrine system in general.

In the endocrine pancreas-specific KO mice, however, the fusion frequency of predocked insulin granules to the plasma membrane was increased. This result suggests that SNAP23 inhibits the fusion of predocked granules in β cells. The SNARE proteins involved in the secretion of predocked insulin granules are syntaxin1A (or syntaxin4), VAMP2, and SNAP25 (Xie et al., 2015). In particular, the syntaxin1A–VAMP2–SNAP25 complex is specific for the fusion of predocked insulin granules (Ohara-Imaizumi et al., 2007). SNAP23 can also bind syntaxin1A and VAMP2. However, the SNAP23–syntaxin1A–VAMP2 complex is less stable (Montana et al., 2009) and less efficient than the SNAP25–syntaxin1A–VAMP2 complex in mediating proteoliposome fusion or dense-core vesicle fusion (Sørensen et al., 2003; Vites et al., 2008). Accordingly, in β cells, the SNAP23–syntaxin1A–VAMP2 complex seems to decrease frequency of insulin granule-to-plasma membrane fusion by competitive inhibition of SNAP25–syntaxin1A–VAMP2 complex formation, consistent with the fact that the SNAP25–syntaxin1A–VAMP2 complex is not formed before stimulation in β cells (Kasai et al., 2012; Takahashi et al., 2015). Thus, SNAP23 depletion leads to increased usage of SNAP25, which subsequently leads to increased fusion of the granules with plasma membranes (Fig. 10). In contrast, in pancreatic acinar cells, expressing only SNAP23, ZG fusion is mediated by SNAP23–syntaxin2–VAMP2 or SNAP23–syntaxin3–VAMP8 complex (Behrendorff et al., 2011; Thorn and Gaisano, 2012), and, at least, the latter complex can fuse proteoliposome (Xu et al., 2015;

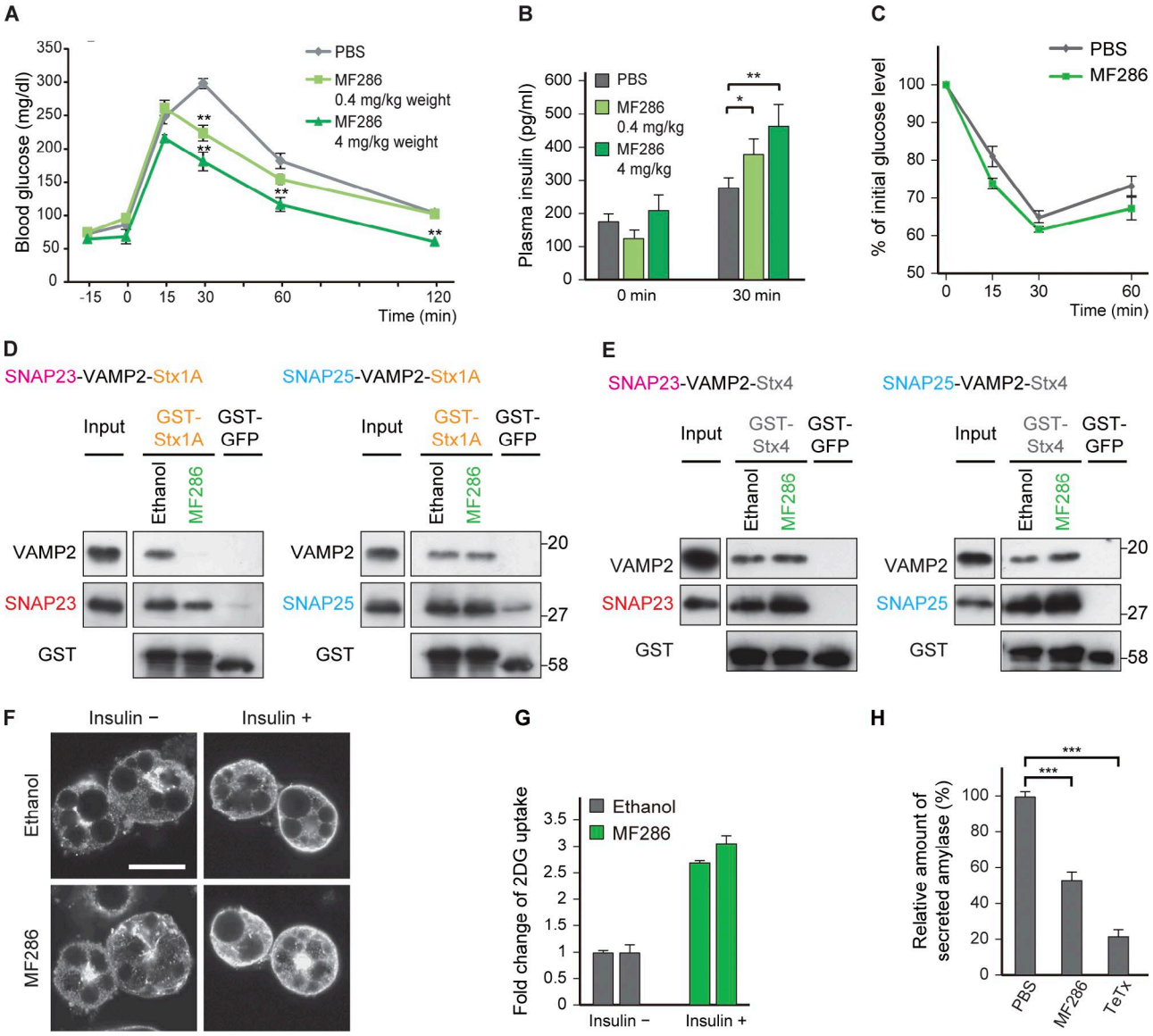

Figure 9. **Effects of MF286 on in vitro SNARE binding and GLUT4 translocation.** (A) Blood glucose concentrations during an IPGTT after injections of PBS or MF286. The data were obtained from four PBS-injected mice and three MF286-injected mice. (B) Plasma insulin concentrations in PBS- or MF286-injected mice without (glucose −) or with (glucose +) glucose stimulation. The data are representative of three independent experiments. (C) Percentages of initial blood glucose concentration during an ITT after injection of PBS or MF286. The data are representative of three independent experiments. (D) In vitro SNARE complex formation among GST–syntaxin1A (Stx1A), His-VAMP2, and His-SNAP23 (left) or GST-Stx1A, His-VAMP2, and His-SNAP25 (right) with or without MF286. (E) In vitro SNARE complex formation among GST-Stx4, His-VAMP2, and His-SNAP23 (left) or GST-Stx4, His-VAMP2, and His-SNAP25 (right) with or without MF286. (F) GLUT4 staining in 3T3-L1 adipocytes before or after insulin stimulation. Bar, 20 µm. (G) Insulin-stimulated glucose uptake in 3T3-L1 adipocytes with or without MF286 treatment. The data are representative of four independent experiments. (H) CCK-stimulated amylase secretion from isolated acinar cells treated with PBS, 37.5 µM MF286, and 300 nM tetanus toxin (TeTx). Tetanus toxin, which cleaves VAMP2 in pancreatic ZGs and inhibits enzyme secretion, was used as a positive control. The data are representative of four independent experiments. Data are mean ± SEM. Significance was calculated by the two-tailed paired Student's *t* test. *, $P < 0.05$; **, $P < 0.01$; ***, $P < 0.001$.

Tadokoro et al., 2016). Thus, fusion activity of SNAP23 is lower than SNAP25, but it seems to be sufficient for ZG-to-plasma membrane fusion in pancreatic acinar cells.

SNAP23 and SNAP25 are spatially segregated in neurons (Suh et al., 2010). Our study showed that, in pancreatic β cells, both SNAP23 and SNAP25 localized to the plasma membranes and acted antagonistically on insulin secretion in vivo. Thus, our study revealed differential secretion mechanisms in pancreatic acini and islets as well as functional differences between SNAP23 and SNAP25 in the same β cells. However, the detailed molecular mechanism for fusion inhibition by SNAP23 remains unclear. Thus, further investigation, including in vitro fusion assay, will be required to address this issue.

Because the steady-state serum insulin levels were within the normal range in the β cell–specific KO mice, we reasoned that SNAP23 inhibitor would be less likely to cause hypoglycemia. Thus, they would be safer drug candidates for diabetes mellitus. We screened a library of small compounds and identified several compounds that bound specifically to SNAP23 but not to SNAP25. One of these compounds, MF286, increased insulin secretion in vitro and in vivo (Figs. 8, 9, and 10). MF286 acts on the last stage of insulin secretion, which is distinct from the stages on

which other drugs act. Thus, MF286 might be a drug candidate for diabetes that could be used in addition to other drugs.

Additionally, MF286 decreased the amylase secretion from pancreatic acinar cells (Fig. 9 H), suggesting that MF286 might also inhibit the formation of the SNAP23–syntaxin2/3–VAMP2/8 complex. Because SNAP23 is involved in the ectopic fusion of ZGs in alcoholic pancreatitis (Cosen-Binker et al., 2008), we expected that MF286 might also be a drug candidate for pancreatitis.

In conclusion, our results demonstrate that SNAP23 is essential for the fusion of ZGs in the pancreatic acini, but it inhibits the fusion of insulin granules in pancreatic β cells. We also demonstrate that MF286, a SNAP23-binding molecule, increases insulin secretion and improves glucose tolerance in vivo. These results suggest the potential of MF286 as a novel drug candidate for the treatment of diabetes and pancreatitis.

Materials and methods

Generation of *Snap23* KO mice

All animal procedures were performed in accordance with the guidelines of the Animal Care and Experimentation Committee of Gunma University and Osaka University. All animals were bred at the Institute of Animal Experience Research of Gunma University and the Institute of Experimental Animal Sciences of Osaka University Medical School.

Snap23 KO mice were generated largely according to previously described methods (Sato et al., 2007). *Snap23* genomic clones were isolated from a mouse bacterial artificial chromosome library (RPCI-22; CHORI) using a 0.6-kb mouse *Snap23* genomic fragment as a probe. Within the targeting vector, a single *loxP* site was inserted into intron 2, and the splice acceptor–internal ribosomal entry site–β-*geo*-poly(A) cassette with two flippase recombinase target sites and one *loxP* site was inserted into intron 5 (Fig. 1 A). This construct was electroporated into embryonic stem cells. Homologous recombinant embryonic stem cells were identified by Southern blot and injected into C57BL/6 to obtain chimeric mice for generation of $Snap23^{geo/+}$ mice. To obtain $Snap23^{-/-}$ mice and *Snap23* floxed mice ($Snap23^{floxed/floxed}$), we crossed $Snap23^{geo/floxed}$ mice with CMV-Cre and Act-Flp-e mice (The Jackson Laboratory), respectively. We crossed *Snap23* floxed mice with Elastase-Cre (Hashimoto et al., 2008), RIP-Cre (Herrera, 2000; Kitamura et al., 2009), or Pdx1-Cre (Gu et al., 2002) mice to generate pancreatic acinar cell– or β cell–specific *Snap23* KO mice. Each mouse line was backcrossed at least 10 times onto a C57BL/6 background. The genotypes of the mice were identified by PCR using the following primers: primer 1 (5′-CTGGGGAATGTGCGTTTG GATGATG-3′), primer 2 (5′-CCCCTTTCATCATGCTTCAAATGC AACC-3′), primer 3 (5′-TGTTCCTGGATTGAGCTCAGGTGGT-3′), primer 4 (5′-AGGTTCGTTCTCTCATGGA-3′), and primer 5 (5′-TCGACCAGTTTAGTTACCC-3′).

Primers 1 and 2, 2 and 3, and 4 and 5 were used for the floxed allele, the null allele, and the *cre* gene, respectively (Fig. 1 A).

Serum biochemistry measurements

Blood samples of each genotype mouse were collected from tail vain after fasting for 18 h. Serum was isolated by centrifugation (3,000 rpm for 15 min). Serum total protein, albumin, blood urea nitrogen, creatinine, sodium, potassium, chloride, calcium, inorganic phosphorus, aspartate aminotransferase, alanine aminotransferase, lactate dehydrogenase, amylase, total cholesterol, triglycerides, high-density lipoprotein (HDL) cholesterol, total bilirubin, and glucose levels were quantified using a 7180 Automatic Analyzer (Hitachi High-Technologies) by the Nagahama Life Science Laboratory.

Light microscopy

For HE staining, 8–12-wk-old mice were intracardially perfused with 3% PFA in 0.1 M phosphate buffer, pH 7.4. The pancreas was removed from each mouse and subjected to additional fixation in the same fixative for 2 h. After fixation, the pancreas was dehydrated in ethanol and embedded in paraffin. Paraffin-embedded pancreatic sections

Table 2. **Serum biochemistries between PBS- or MF286-injected wild-type mice**

	0 d		30 d	
	PBS	MF286	PBS	MF286
Age (wk)	8	8	12	12
n	3	3	3	3
Total protein (g/dl)	5.3 ± 0.13	5.1 ± 0.07	5.3 ± 0.07	5.5 ± 0.07
Albumin (g/dl)	3.8 ± 0.12	4.1 ± 0.07	4.0 ± 0.12	4.3 ± 0.07
Blood urea nitrogen (mg/dl)	27.1 ± 1.69	32.7 ± 4.57	25.7 ± 1.1	29.0 ± 1.8
Creatinine (mg/dl)	0.1 ± 0.007	0.2 ± 0.01	0.1 ± 0.07	0.1 ± 0.07
Na (mEq/l)	152.7 ± 1.33	154.7 ± 0.67	152.0 ± 0.0	152.0 ± 0.0
K (mEq/l)	6.0 ± 0.12	5.5 ± 0.13	5.7 ± 0.47	5.5 ± 0.37
Cl (mEq/l)	100.7 ± 1.33	102.0 ± 0.0	100.0 ± 0.0	99.3 ± 0.7
Ca (mEq/l)	9.3 ± 0.18	9.1 ± 0.13	9.0 ± 0.0	9.1 ± 0.07
Inorganic phosphorus (mg/dl)	6.2 ± 0.72	6.1 ± 0.07	6.1 ± 0.7	5.8 ± 0.4
Aspartate aminotransferase (IU/l)	66.0 ± 7.2	62.0 ± 3.1	59.3 ± 2.4	60.7 ± 2.9
Alanine aminotransferase (IU/l)	22.0 ± 3.05	23.3 ± 2.7	18.7 ± 0.7	20.0 ± 1.2
Lactate dehydrogenase (IU/l)	272.0 ± 17.3	233.3 ± 11.4	276.7 ± 26.4	276.0 ± 51.2
Amylase (IU/l)	4,696.0 ± 1,332.6	4,894.0 ± 842.2	4,031.3 ± 1,644.4	3,004.0 ± 222.3
Total cholesterol (mg/dl)	82.7 ± 10.9	75.3 ± 4.8	90.0 ± 2.3	84.7 ± 3.5
Triglycerides (mg/dl)	36.7 ± 7.1	36.0 ± 3.1	67.3 ± 15.2	40.7 ± 5.7
HDL cholesterol (mg/dl)	46.7 ± 7.9	36.7 ± 2.9	44.7 ± 0.7	43.3 ± 2.9
Total bilirubin (mg/dl)	0.1 ± 0.01	0.1 ± 0.07	0.1 ± 0.01	0.1 ± 0.01
Glucose (mg/dl)	97.3 ± 5.5	112.7 ± 6.4	110.0 ± 11.5	119.3 ± 4.8

Data are mean ± SEM unless otherwise noted.

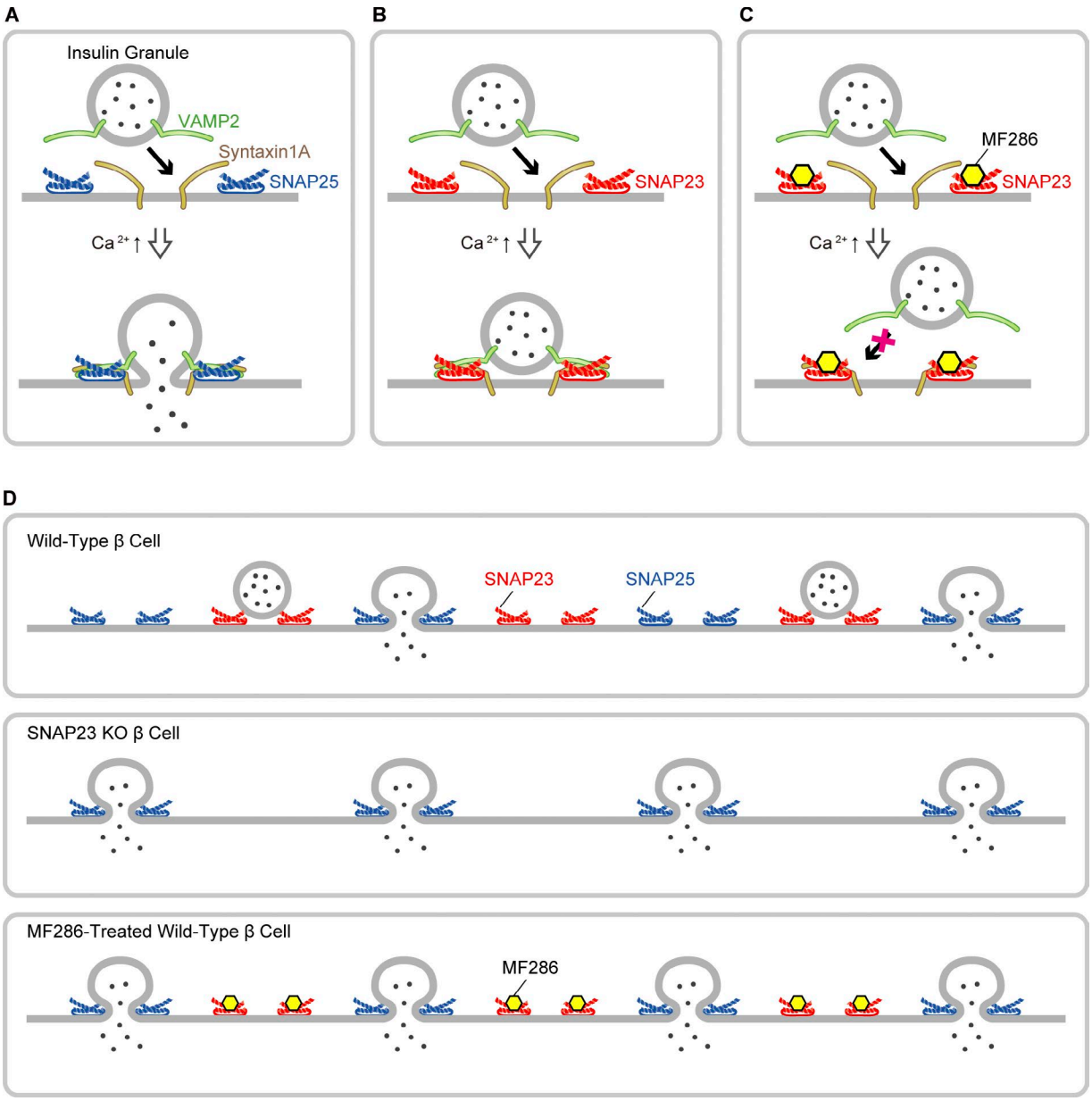

Figure 10. **Schematic diagrams showing the roles of SNAP23 in pancreatic β cells.** (A) SNAP25 forms a complex with syntaxin1A and VAMP2, which allows insulin granules to effectively dock and fuse at the plasma membrane. (B) The SNAP23–syntaxin1A–VAMP2 complex has a weaker ability to fuse insulin granules at the plasma membrane. Thus, the existence of SNAP23 will obstruct the insulin secretion by SNAP25. (C) MF286 blocks SNAP23 to form a complex with syntaxin1A and VAMP2. (D) In wild-type cells (top), both SNAP23 and SNAP25 are expressed and localized at the plasma membrane. SNAP23 and SNAP25 compete with each other for binding to syntaxin1A and VAMP2. Because the SNAP25–syntaxin1A–VAMP2 complex is more efficient in exocytosis, SNAP23 acts as a competitive inhibitor of insulin secretion. In contrast, depletion (middle) or inhibition (bottom) of SNAP23 results in an increase in the SNAP25–syntaxin1A–VAMP2 complex. Therefore, secretion of insulin is increased. For simplification, syntaxin1A and VAMP2 are not presented in this scheme.

(4 µm) were stained with a solution of HE. For immunohistochemistry, paraffin-embedded sections of human pancreas were purchased from BioChain Institute, Inc. The sections were labeled using primary and secondary antibodies as described in the Antibodies section after antigen retrieval (autoclaved in citrate buffer). For immunofluorescence microscopy, cryoprotection was performed after fixation by incubating the tissues consecutively in 4, 10, 15, and 20% sucrose in 0.1 M phosphate buffer, pH 7.4. The tissues were embedded in O.C.T. compound (Sakura) and then frozen in liquid nitrogen–chilled isopentane. The frozen sections were cut using a CM3000 cryostat (Leica Biosystems) and labeled with primary and secondary antibodies as described in the Antibodies section. Confocal images were obtained using an FV1000D laser-scanning microscope (Olympus) with a UPlanSApo 60× objective lens (NA 1.35; Olympus).

Antibodies

The anti-SNAP23 polyclonal antibody was raised against a purified recombinant His6-SNAP23 protein according to previously described protocols (Chen et al., 1999). Rabbits were immunized with purified His6-SNAP23. The resulting serum was purified by passage through an affinity column with GST-SNAP25. The serum was further purified by affinity chromatography with GST-SNAP23.

The following primary antibodies were used: SNAP25 (mouse; SMI-81; Covance), SNAP25 (rabbit; 5308; Cell Signaling Technology), syntaxin1A (mouse; S0664; Sigma-Aldrich), VAMP2 (mouse; 104211; Synaptic Systems), VAMP2 (rabbit; 13508; Cell Signaling Technology), GP2 (mouse; 2F11-C3; MBL International Corporation), GAPDH (mouse; CB1001; EMD Millipore), and GLUT4 (provided by H. Shibata, Institute for Molecular and Cellular Regulation, Gunma University, Gunma, Japan; Shibata et al., 1995). The anti-GST rabbit polyclonal antibody was raised against a purified GST protein, and the antiserum was affinity purified with a GST column. For secondary antibodies, EnVision+ System HRP-labeled polymer anti-rabbit and anti-mouse (Dako) and Alexa Fluor 488–, 568–, and 594–labeled donkey anti–rabbit and anti–mouse IgG (Molecular Probes) were used.

Western blot analysis

Tissues or cells were homogenized in lysis buffer (80 mM Tris-HCl, pH 6.8, and 2% SDS) containing a protease inhibitor cocktail (Nacalai Tesque, Inc.); the lysates were subsequently boiled and centrifuged at 20,000 *g* for 10 min. The supernatants were used for SDS-PAGE. The antibodies noted in the previous section were used as primary antibodies. HRP-labeled donkey anti-mouse and anti-rabbit antibodies (Jackson ImmunoResearch Laboratories, Inc.) were used as secondary antibodies. An Immobilon Western Chemiluminescent HRP Substrate kit (EMD Millipore) was used for detection. Chemiluminescent images were obtained using an automatic film developer.

Electron microscopy

For electron microscopy, 8–12-wk-old control, AcKO, or PcKO mice were used. CCK (0.25 µg/kg weight) or glucose (1 g/kg weight) was administered by i.p. injection. 30 min after the injections, the mice were perfused intracardially with 2.5% glutaraldehyde and 2% PFA in 0.1 M cacodylate buffer, pH 7.4. The pancreas was removed from each mouse and fixed in the same fixative and 0.1% OsO_4, after which it was further fixed in 0.5% uranyl acetate in H_2O, dehydrated, and embedded in Quetol 812 (Nisshin EM). Ultrathin sections were cut using an ultra-microtome (Reichert Jung). Electron micrographs were taken using a JEM-1010 (JEOL).

Colorimetric assay for amylase and fecal triglyceride

Acinar cells were isolated from control and AcKO mice as previously described (Nemoto et al., 2001). The isolated acinar cells were incubated with or without 100 pM CCK for 1 h at 37°C. Secreted amylase from the acinar cells was measured using a QuantiChrom Alpha-Amylase Assay kit (BioAssay Systems) according to the manufacturer's instructions.

For extraction of lipids, stools were homogenized with chloroform/methanol (2:1). The homogenate was centrifuged, and the lipid-containing chloroform layer was collected. The solvent was mixed with 0.36 M $CaCl_2$ in methanol, and the chloroform layer was collected again after centrifugation. Chloroform was evaporated, and remaining lipids were used for quantification. Triglycerides were measured using a Triglyceride E-Test Wako (Wako Pure Chemical Industries) according to the manufacturer's instructions.

Parotid acinar cell culture and real-time PCR

Primary parotid acinar cell culture was performed as previously described (Fujita-Yoshigaki et al., 2005). Parotid acinar cells were isolated from *Snap23* floxed mice (*Snap23*$^{floxed/floxed}$) and infected with LacZ- or Cre-expressing adenovirus for 48 h. After infection, cells were stimulated with 1 µM IPR and 10 µM MeCh for 15 min at 37°C. Secreted amylase in the supernatant was quantified using colorimetric assay. Total RNA was extracted from acinar cells using a NucleoSpin RNA kit (Macherey-Nagel) according to the manufacturer's instructions. First-strand cDNA was synthesized by random primers (6-mers) and reverse transcription (Takara Bio Inc.). Real-time PCR was performed using ViiA7 (Applied Biosystems). Universal Probes 13 and 78 (Roche) were used for SNAP23 and glucose-6-phosphate dehydrogenase X-linked (G6PDX), respectively. The primers used for PCR were as follows: SNAP23 sense (5′-CACTATGCTGGATGAGCAAGG-3′), SNAP23 antisense (5′-CAACACTTGTTGAGTTCTGTTAAAGTC-3′), G6PDX sense (5′-GAAAGCAGAGTGAGCCCTTC-3′), and G6PDX antisense (5′-CATAGGAATTACGGGCAAGA-3′).

Two-photon excitation imaging

The isolation of pancreatic acinar cells and β cells was described previously (Nemoto et al., 2001; Takahashi et al., 2002). ZG exocytosis in the control and AcKO acinar cells or insulin granule exocytosis in the control and PcKO β cells was visualized using a solution that contained 0.5 or 0.7 mM SRB as a fluid-phase tracer. Two-photon excitation imaging for pancreatic acinar cells was performed using a laser-scanning microscope (A1R MP+; Nikon) with an XLPLan 25× objective lens (NA 1.05; Olympus) and a femtosecond laser (Mai Tai eHP DeepSee; Spectra-Physics). For pancreatic β cells, two-photon imaging was performed using an inverted laser-scanning microscope (FV1000 and IX81; Olympus) equipped with a water-immersion objective lens (UPlanApo 60× W/IR; NA 1.2; Olympus) and a femtosecond laser (Mai Tai; Spectra-Physics). Exocytosis was measured in response to 100 pM CCK or 20 mM glucose within arbitrary areas of the isolated acinar cells and islets. Increases in the cytosolic Ca^{2+} concentration were measured using the Fura-2 AM (K_{Ca}: 0.2 µM) or Fura-2 FF (K_{Ca}: 40 µM) Ca^{2+} indicator and were reported as $(F_0 - F)/F_0$, where F_0 and F represent the resting and post-stimulation fluorescence levels, respectively.

IPGTT, ITT, and measurement of plasma insulin concentration

The IPGTT, ITT, and measurement of plasma insulin concentration were performed as described previously (Gomi et al., 2005). Blood glucose concentrations in control, BcKO, or PcKO mice were measured at 15, 30, 60, and 120 min after glucose or insulin (Humalin R; Eli Lilly and Company) injection (1 g/kg or 0.75 U/kg weight) with ACCU-CHEK (Roche) or Glutest Neo Super (Sanwa Kagaku Kenkyusho). To measure plasma insulin concentration, plasma samples were obtained from control or BcKO mice at 0, 15, 30, and 60 min after glucose injections. An LBIS mouse insulin ELISA kit (Shibayagi) was used according to the manufacturer's instructions.

Islet preparation and insulin release assay

Pancreatic islets were isolated from control and BcKO mice by collagenase digestion, as previously described (Ohara-Imaizumi et al., 2004). For the batch incubation assay, 10 size-matched islets were preincubated for 30 min in Krebs-Ringer buffer (KRB) containing 110 mM NaCl, 4.4 mM KCl, 1.45 mM KH_2PO_4, 1.2 mM $MgSO_4$, 2.3 mM calcium gluconate, 4.8 mM $NaHCO_3$, 2.2 mM glucose, 10 mM Hepes, pH 7.4, and 0.3% BSA and then transferred into 1 ml KRB containing 2.2 or 16.7 mM glucose. After 30-min incubation, 200 µl supernatant was recovered as the secreted insulin sample. For the perfusion assay, 40 size-matched islets were housed in a small chamber and perifused with KRB containing 2.8 mM glucose for 30 min at a flow rate of 0.5 ml/min, and insulin release was stimulated by 22 mM glucose for 30 min. After the experiments, islets were solubilized by 1% Triton X-100 and sonicated on ice to recover the total cellular content of insulin. The secreted insulin and total cellular content of insulin were measured using an insulin ELISA kit (Morinaga Institute of Biological Science, Inc.).

TIRFM

The isolated islets from control and BcKO mice were dispersed and cultured on fibronectin-coated high-refractive index cover glass (Olympus) in RPMI 1640 medium (Gibco) supplemented with 10% FBS (Gibco), 200 U/ml penicillin, and 200 µg/ml streptomycin at 37°C in an atmosphere of 5% CO_2 (Ohara-Imaizumi et al., 2007). To label insulin secretory granules, β cells were infected with recombinant adenovirus Adex1CA insulin-GFP. Experiments were performed 18–24 h after the final infection. A total internal reflection system with a high-aperture objective lens (Apo 100× OHR; NA 1.65; Olympus) was used as previously described (Ohara-Imaizumi et al., 2007). In brief, β cells expressing insulin-GFP on the cover glass were mounted in an open chamber and incubated for 30 min with KRB. Cells were then transferred to a thermostat-controlled stage (37°C) and stimulated with 22 mM glucose. TIRF images in live cells were acquired every 300 ms after glucose stimulation. The data analysis was performed using Metamorph software (Universal Imaging). The number of fusion events per cell was manually counted. The exocytotic fusion events in each corresponding cell were counted during a time course.

SNARE binding assay

The in vitro SNARE binding assay was performed as previously described (Pevsner et al., 1994). Full-length human Syntaxin1A cDNA, inserted into the pET-41 Ek/LIC vector (provided by J. Mima, Institute for Protein Research, Osaka University, Osaka, Japan), was used to generate the recombinant GST-Syntaxin1A protein. The cytoplasmic region of mouse syntaxin4 inserted into the pGEX-6P-1 vector was used to generate the recombinant GST–syntaxin4 protein. Full-length mouse SNAP25 cDNA and cDNA containing the cytoplasmic region of mouse VAMP2 were subcloned into the pQE32 vector (QIAGEN) to generate the recombinant His-SNAP25 and His-VAMP2 proteins, respectively. All recombinant proteins, except GST-Syntaxin4, were expressed in Rosetta2 *Escherichia coli* as His6-tagged fusion proteins and purified using Ni-NTA agarose (QIAGEN) according to the manufacturer's instructions. GST-Syntaxin4 was expressed in Rosetta2 *E. coli* as a GST-tagged fusion protein and purified with Glutathione Sepharose 4B (GE Healthcare) according to the manufacturer's instructions.

For the binding competition experiment, His-SNAP23 (0, 0.6, 5, and 10 µM), His-Stx1A, and His-VAMP2 (0.6 µM each) were mixed in buffer (150 mM NaCl, 20 mM Tris-HCl, pH 7.5, 1 mM EDTA, and 5% glycerol) and incubated for 2 h at 4°C. The mixture was combined with GST-SNAP25 (0.6 µM) and Glutathione Sepharose 4B (GE Healthcare) and rotated overnight at 4°C. The glutathione beads were washed three times in wash buffer (300 mM NaCl, 20 mM Tris-HCl, pH 7.5, 1 mM EDTA, 5% glycerol, and 0.1% Triton X-100) and subjected to microcentrifugation for 30 s at 4°C. The beads were boiled and analyzed by SDS-PAGE and immunoblotting.

For the MF286 experiment, His-SNAP23 or His-SNAP25 was incubated with ethanol or MF286 (2 µM) for 1 h at 4°C. Next, 0.6 µM each of His-SNAP23 or His-SNAP25, His-VAMP2, and GST-Syntaxin1A or GST-Syntaxin4 was combined in buffer (150 mM NaCl, 20 mM Tris-HCl, pH 7.5, 1 mM EDTA, and 5% glycerol) with ethanol or 2 µM MF286 and rotated with Glutathione Sepharose 4B (GE Healthcare) overnight at 4°C. The glutathione beads were washed three times in wash buffer and subjected to microcentrifugation for 30 s at 4°C. The beads were boiled and analyzed by SDS-PAGE and immunoblotting.

Immunoprecipitation

Immunoprecipitation was performed as previously described (Oh and Thurmond, 2009). Isolated islets from control and BcKO mice or MIN6 cells (provided by J. Miyazaki, Osaka University, Osaka, Japan) were preincubated for 30 min in glucose-free modified Krebs ringer bicarbonate buffer (5 mM KCl, 120 mM NaCl, 15 mM Hepes, pH 7.4, 24 mM $NaHCO_3$, 1 mM $MgCl_2$, 2 mM $CaCl_2$, and 1 mg/ml BSA) with 1 mM *N*-ethylmaleimide. The islets were additionally incubated with 25 mM glucose for 15 min. The islets or MIN6 cells were lysed in NP-40 lysis buffer (1% NP-40, 25 mM Hepes, pH 7.4, 10% glycerol, 137 mM NaCl, and protease inhibitor cocktail), and the lysates were subsequently cleared by microcentrifugation for 10 min at 4°C. A total of 10 mg of cleared lysate was used for immunoprecipitation with the appropriate antibodies. The precipitated products were boiled and analyzed by SDS-PAGE and immunoblotting. Rabbit TrueBlot HRP-anti rabbit antibody (Rockland Immunochemicals) was used for the detection of SNAP25 or SNAP23 in the immunoprecipitate from the lysate.

Cell culture and siRNA knockdown of SNAP23 or SNAP25 expression

MIN6 cells were cultured in DMEM (Wako Pure Chemical Industries) supplemented with 10% FCS and 0.0005% β-mercaptoethanol at 37°C under a 5% CO_2/95% air atmosphere.

For SNAP23 or SNAP25 knockdown, the following Ambion silencer siRNAs (Thermo Fisher Scientific) were transfected with Lipofectamine RNAiMAX (Invitrogen): control siRNA (AM4611), SNAP23 siRNA (64778; 5′-GGCAUGGACCAAAUAAAUATT-3′), and SNAP25 siRNA (151786; 5′-GCAACAACUACGCAUGCUCTT-3′).

Measurement of hGH secretion

The hGH-expressing MIN6 cells were washed three times with KRB. After washing, the cells were incubated with KRB plus 0.3% BSA and stimulated with KRB plus 30 mM KCl. At the experimental endpoint, 1 ml of chilled 1% (vol/vol) NP-40 was added, and the samples were sonicated (UR-20P; Tomy Seiko Co.) on ice. Secreted hGH and the total cellular content of hGH were measured using an hGH ELISA kit (Roche).

Chemical array screening of SNAP23-binding compounds

Chemical array screening was performed as previously described (Hagiwara et al., 2010; Zimmermann et al., 2013). Eight array slides that included 23,275 compounds were incubated with 2 µM GST-SNAP23 or 500 µl GST-SNAP25 solution for 1 h at 30°C in the following buffer: 10 mM Tris-HCl, 150 mM NaCl, 0.05% Tween 20, and 1% skim milk, pH 8. After washing, the array slides were incubated with anti-GST antibody for 1 h at 30°C. This incubation was followed by another wash step and incubation with a Cy5-conjugated secondary antibody for 1 h at 30°C. After a final wash step, the slides were scanned at 635 nm using a GenePix 4300A microarray scanner (Molecular Devices). The compounds that bound SNAP23 were identified by the fluorescence intensity of each spot.

Treatment of MIN6 cells, isolated islets, and acini with chemical compounds and injection of mice with MF286

MIN6 cells that had been cultured in 96-well plates were incubated overnight with chemical compounds (3, 10, and 30 µg/ml). MIN6 cell viability was measured after the compound treatments using Cell Count Reagent SF (Nacalai Tesque, Inc.) according to the manufacturer's instructions. Isolated islets from wild-type mice were incubated with MF286 (0, 0.001, 0.01, 0.1, 1, and 10 µM) for 1 h. To measure secreted insulin, the islets or MIN6 cells were washed three times with KRB plus 2.2 or 2.8 mM glucose. After washing, they were incubated with KRB and subsequently stimulated with KRB plus 22 or 13.9 mM glucose for 1 h. A rat Insulin RIA kit (EMD Millipore) or an LBIS mouse insulin ELISA kit (Shibayagi) was used to measure insulin according to the manufacturer's instructions.

Isolated acinar cells from wild-type mice were incubated with MF286 (37.5 µM) or 300 nM tetanus toxin (Sigma-Aldrich) for 1 h at

37°C, as previously described (Rosado et al., 2005). Cells were then stimulated by 100 pM CCK for 1 h at 37°C. Secreted amylase from the acinar cells was measured using a QuantiChrom Alpha-Amylase Assay kit (BioAssay Systems) according to the manufacturer's instructions.

For studying the in vivo effect, MF286 was injected i.p. (0.4 or 4 mg/kg weight) into 8-wk-old female C57BL/6 mice. IPGTT, ITT, and plasma insulin were measured at 15 or 30 min after MF286 injection as described in IPGTT, ITT, and measurement of plasma insulin concentration.

SPR analysis

MF286 and DS565-8 (10 mM each) were spotted and immobilized onto the sensor chip (gold-coated glass slide; PBA-CS-03-5; Plexera) by UV cross-linking. Purified His-SNAP23 or His-SNAP25 protein in running buffer (150 mM NaCl, 20 mM Tris-HCl, pH 7.5, 1 mM EDTA, and 5% glycerol) was loaded at 30°C. The changes in reflected light intensity were recorded and displayed as a sensorgram using a PlexArray HT Analyzer (Plexera).

2-Deoxyglucose uptake into 3T3-L1 adipocytes

The adipogenesis of 3T3-L1 fibroblasts was induced by treatment with insulin, dexamethasone, and isobutylmethylxanthine as described previously (Kawanishi et al., 2000). 3T3-L1 adipocytes were incubated with or without MF286 (37.5 µM) for 2 h. The 2-deoxyglucose incorporated into 3T3-L1 adipocytes was measured using a 2-DG Uptake Measurement kit (Cosmo Bio) according to the manufacturer's instructions.

Online supplemental material

Fig. S1 shows coimmunostaining of SNAP23 and insulin, glucagon, and somatostatin in pancreatic islets from control, BcKO, and PcKO mice. Fig. S2 shows coimmunostaining of SNAP25 and insulin, glucagon, and somatostatin in pancreatic islets from control, BcKO, and PcKO mice. Fig. S3 shows glucose tolerance and insulin secretion in PcKO mice. Fig. S4 shows IPGTT and plasma insulin concentration in BcKO mice with or without MF286. Fig. S5 shows the effect of long-term administration of MF286. Video 1 shows two-photon imaging of exocytotic events in control and AcKO acinar cells. Video 2 shows two-photon imaging of exocytotic events in control and PcKO islets.

Acknowledgments

We thank M. Takano, T. Akuzawa, K. Inami, T. Horie, Y. Okada, R. Hirai, H. Kobayashi, H. Hata, N. Atik, M. Taniguchi, A. Goto, H. Togawa, A. Watanabe, Y. Noguchi, A Koizumi, T. Saito, and K. Honda for technical assistance; D. C. Thurmond, M. Sato, T. Sobajima, M. Inoue, and T. Hara for advice; J. Miyazaki for providing the MIN6 cells; J. Mima for advice and for providing the human syntaxin1A cDNA construct; and H. Shibata for providing the GLUT4 antibody. The PlexArray HT Analyzer was lent by the Division of Innovative Research for Drug Development, Osaka University Institute for Academic Initiatives.

This work was supported by Grants-in-Aid for the 21st Century Center of Excellence Program of the Japanese Ministry of Education, Culture, Sports, Science, and Technology (to K. Sato and A. Harada), Grants-in-Aid for Scientific Research from the Japan Society for the Promotion of Science (KAKENHI grants JP24390046 to A. Harada and JP26870335 to M. Kunii),the Daiwa Securities Health Foundation, the Suzuken Memorial Foundation (to T. Sato), the Daiichi Sankyo Foundation of Life Science, Novartis Foundation (Japan) for the Promotion of Science (to A. Harada), The Uehara Memorial Foundation (to S. Yoshimura), and the joint research program of the Institute for Molecular and Cellular Regulation, Gunma University.

The authors declare no competing financial interests.

Author contributions: M. Kunii, M. Ohara-Imaizumi, N. Takahashi, M. Kobayashi, R. Kawakami, Y. Kondoh, T. Shimizu, S. Simizu, B. Lin, K. Nunomura, K. Aoyagi, M. Ohno, M. Ohmuraya, T. Sato, S. Yoshimura, K. Sato, R. Harada, Y.-J. Kim, H. Osada, T. Nemoto, H. Kasai, T. Kitamura, S. Nagamatsu, and A. Harada conducted the experiments. A. Harada supervised the project. M. Kunii, R. Harada, and A. Harada wrote the manuscript.

Submitted: 7 April 2016
Accepted: 26 August 2016

References

Abonyo, B.O., D. Gou, P. Wang, T. Narasaraju, Z. Wang, and L. Liu. 2004. Syntaxin 2 and SNAP-23 are required for regulated surfactant secretion. *Biochemistry.* 43:3499–3506. http://dx.doi.org/10.1021/bi036338y

Behrendorff, N., S. Dolai, W. Hong, H.Y. Gaisano, and P. Thorn. 2011. Vesicle-associated membrane protein 8 (VAMP8) is a SNARE (soluble *N*-ethylmaleimide-sensitive factor attachment protein receptor) selectively required for sequential granule-to-granule fusion. *J. Biol. Chem.* 286:29627–29634. http://dx.doi.org/10.1074/jbc.M111.265199

Chen, D., S.L. Minger, W.G. Honer, and S.W. Whiteheart. 1999. Organization of the secretory machinery in the rodent brain: distribution of the t-SNAREs, SNAP-25 and SNAP-23. *Brain Res.* 831:11–24. http://dx.doi.org/10.1016/S0006-8993(99)01371-2

Cosen-Binker, L.I., M.G. Binker, C.C. Wang, W. Hong, and H.Y. Gaisano. 2008. VAMP8 is the v-SNARE that mediates basolateral exocytosis in a mouse model of alcoholic pancreatitis. *J. Clin. Invest.* 118:2535–2551. http://dx.doi.org/10.1172/JCI34672

Freedman, S.J., H.K. Song, Y. Xu, Z.Y.J. Sun, and M.J. Eck. 2003. Homotetrameric structure of the SNAP-23 N-terminal coiled-coil domain. *J. Biol. Chem.* 278:13462–13467. http://dx.doi.org/10.1074/jbc.M210483200

Fujita-Yoshigaki, J., A. Tagashira, T. Yoshigaki, S. Furuyama, and H. Sugiya. 2005. A primary culture of parotid acinar cells retaining capacity for agonists-induced amylase secretion and generation of new secretory granules. *Cell Tissue Res.* 320:455–464. http://dx.doi.org/10.1007/s00441-005-1076-x

Gomi, H., S. Mizutani, K. Kasai, S. Itohara, and T. Izumi. 2005. Granuphilin molecularly docks insulin granules to the fusion machinery. *J. Cell Biol.* 171:99–109. http://dx.doi.org/10.1083/jcb.200505179

Gu, G., J. Dubauskaite, and D.A. Melton. 2002. Direct evidence for the pancreatic lineage: NGN3+ cells are islet progenitors and are distinct from duct progenitors. *Development.* 129:2447–2457.

Hagiwara, K., Y. Kondoh, A. Ueda, K. Yamada, H. Goto, T. Watanabe, T. Nakata, H. Osada, and Y. Aida. 2010. Discovery of novel antiviral agents directed against the influenza A virus nucleoprotein using photo-cross-linked chemical arrays. *Biochem. Biophys. Res. Commun.* 394:721–727. http://dx.doi.org/10.1016/j.bbrc.2010.03.058

Hashimoto, D., M. Ohmuraya, M. Hirota, A. Yamamoto, K. Suyama, S. Ida, Y. Okumura, E. Takahashi, H. Kido, K. Araki, et al. 2008. Involvement of autophagy in trypsinogen activation within the pancreatic acinar cells. *J. Cell Biol.* 181:1065–1072. http://dx.doi.org/10.1083/jcb.200712156

Heffner, C.S., C. Herbert Pratt, R.P. Babiuk, Y. Sharma, S.F. Rockwood, L.R. Donahue, J.T. Eppig, and S.A. Murray. 2012. Supporting conditional mouse mutagenesis with a comprehensive cre characterization resource. *Nat. Commun.* 3:1218. http://dx.doi.org/10.1038/ncomms2186

Herrera, P.L. 2000. Adult insulin- and glucagon-producing cells differentiate from two independent cell lineages. *Development.* 127:2317–2322.

Hong, W. 2005. SNAREs and traffic. *Biochim. Biophys. Acta.* 1744:493–517. http://dx.doi.org/10.1016/j.bbamcr.2005.03.014

Hong, W., and S. Lev. 2014. Tethering the assembly of SNARE complexes. *Trends Cell Biol.* 24:35–43. http://dx.doi.org/10.1016/j.tcb.2013.09.006

Hou, J.C., L. Min, and J.E. Pessin. 2009. Insulin granule biogenesis, trafficking and exocytosis. *Vitam. Horm.* 80:473–506. http://dx.doi.org/10.1016/S0083-6729(08)00616-X

Jahn, R., and R.H. Scheller. 2006. SNAREs--engines for membrane fusion. *Nat. Rev. Mol. Cell Biol.* 7:631–643. http://dx.doi.org/10.1038/nrm2002

Kasai, H., N. Takahashi, and H. Tokumaru. 2012. Distinct initial SNARE configurations underlying the diversity of exocytosis. *Physiol. Rev.* 92:1915–1964. http://dx.doi.org/10.1152/physrev.00007.2012

Kawanishi, M., Y. Tamori, H. Okazawa, S. Araki, H. Shinoda, and M. Kasuga. 2000. Role of SNAP23 in insulin-induced translocation of GLUT4 in 3T3-L1 adipocytes. Mediation of complex formation between syntaxin4 and VAMP2. *J. Biol. Chem.* 275:8240–8247. http://dx.doi.org/10.1074/jbc.275.11.8240

Kitamura, T., Y.I. Kitamura, M. Kobayashi, O. Kikuchi, T. Sasaki, R.A. Depinho, and D. Accili. 2009. Regulation of pancreatic juxtaductal endocrine cell formation by FoxO1. *Mol. Cell. Biol.* 29:4417–4430. http://dx.doi.org/10.1128/MCB.01622-08

Montana, V., W. Liu, U. Mohideen, and V. Parpura. 2009. Single molecule measurements of mechanical interactions within ternary SNARE complexes and dynamics of their disassembly: SNAP25 vs. SNAP23. *J. Physiol.* 587:1943–1960. http://dx.doi.org/10.1113/jphysiol.2009.168575

Nemoto, T., R. Kimura, K. Ito, A. Tachikawa, Y. Miyashita, M. Iino, and H. Kasai. 2001. Sequential-replenishment mechanism of exocytosis in pancreatic acini. *Nat. Cell Biol.* 3:253–258. http://dx.doi.org/10.1038/35060042

Oh, E., and D.C. Thurmond. 2009. Munc18c depletion selectively impairs the sustained phase of insulin release. *Diabetes.* 58:1165–1174. (published erratum appears in *Diabetes*. 2010. 59:756) http://dx.doi.org/10.2337/db08-1059

Ohara-Imaizumi, M., C. Nishiwaki, T. Kikuta, S. Nagai, Y. Nakamichi, and S. Nagamatsu. 2004. TIRF imaging of docking and fusion of single insulin granule motion in primary rat pancreatic beta-cells: different behaviour of granule motion between normal and Goto-Kakizaki diabetic rat beta-cells. *Biochem. J.* 381:13–18. http://dx.doi.org/10.1042/BJ20040434

Ohara-Imaizumi, M., T. Fujiwara, Y. Nakamichi, T. Okamura, Y. Akimoto, J. Kawai, S. Matsushima, H. Kawakami, T. Watanabe, K. Akagawa, and S. Nagamatsu. 2007. Imaging analysis reveals mechanistic differences between first- and second-phase insulin exocytosis. *J. Cell Biol.* 177:695–705. http://dx.doi.org/10.1083/jcb.200608132

Pevsner, J., S.-C. Hsu, J.E.A. Braun, N. Calakos, A.E. Ting, M.K. Bennett, and R.H. Scheller. 1994. Specificity and regulation of a synaptic vesicle docking complex. *Neuron.* 13:353–361. http://dx.doi.org/10.1016/0896-6273(94)90352-2

Pickett, J.A., and J.M. Edwardson. 2006. Compound exocytosis: mechanisms and functional significance. *Traffic.* 7:109–116. http://dx.doi.org/10.1111/j.1600-0854.2005.00372.x

Ravichandran, V., A. Chawla, and P.A. Roche. 1996. Identification of a novel syntaxin- and synaptobrevin/VAMP-binding protein, SNAP-23, expressed in non-neuronal tissues. *J. Biol. Chem.* 271:13300–13303. http://dx.doi.org/10.1074/jbc.271.23.13300

Reales, E., F. Mora-López, V. Rivas, A. García-Poley, J.A. Brieva, and A. Campos-Caro. 2005. Identification of soluble *N*-ethylmaleimide-sensitive factor attachment protein receptor exocytotic machinery in human plasma cells: SNAP-23 is essential for antibody secretion. *J. Immunol.* 175:6686–6693. http://dx.doi.org/10.4049/jimmunol.175.10.6686

Regazzi, R., C.B. Wollheim, J. Lang, J.-M. Theler, O. Rossetto, C. Montecucco, K. Sadoul, U. Weller, M. Palmer, and B. Thorens. 1995. VAMP-2 and cellubrevin are expressed in pancreatic β-cells and are essential for Ca^{2+}-but not for GTP gamma S-induced insulin secretion. *EMBO J.* 14:2723–2730.

Rosado, J.A., P.C. Redondo, G.M. Salido, S.O. Sage, and J.A. Pariente. 2005. Cleavage of SNAP-25 and VAMP-2 impairs store-operated Ca^{2+} entry in mouse pancreatic acinar cells. *Am. J. Physiol. Cell Physiol.* 288:C214–C221. http://dx.doi.org/10.1152/ajpcell.00241.2004

Sadoul, K., J. Lang, C. Montecucco, U. Weller, R. Regazzi, S. Catsicas, C.B. Wollheim, and P.A. Halban. 1995. SNAP-25 is expressed in islets of Langerhans and is involved in insulin release. *J. Cell Biol.* 128:1019–1028. http://dx.doi.org/10.1083/jcb.128.6.1019

Sadoul, K., A. Berger, H. Niemann, U. Weller, P.A. Roche, A. Klip, W.S. Trimble, R. Regazzi, S. Catsicas, and P.A. Halban. 1997. SNAP-23 is not cleaved by botulinum neurotoxin E and can replace SNAP-25 in the process of insulin secretion. *J. Biol. Chem.* 272:33023–33027. http://dx.doi.org/10.1074/jbc.272.52.33023

Sato, T., S. Mushiake, Y. Kato, K. Sato, M. Sato, N. Takeda, K. Ozono, K. Miki, Y. Kubo, A. Tsuji, et al. 2007. The Rab8 GTPase regulates apical protein localization in intestinal cells. *Nature.* 448:366–369. http://dx.doi.org/10.1038/nature05929

Shibata, H., Y. Suzuki, W. Omata, S. Tanaka, and I. Kojima. 1995. Dissection of GLUT4 recycling pathway into exocytosis and endocytosis in rat adipocytes. Evidence that GTP-binding proteins are involved in both processes. *J. Biol. Chem.* 270:11489–11495. http://dx.doi.org/10.1074/jbc.270.19.11489

Sørensen, J.B., G. Nagy, F. Varoqueaux, R.B. Nehring, N. Brose, M.C. Wilson, and E. Neher. 2003. Differential control of the releasable vesicle pools by SNAP-25 splice variants and SNAP-23. *Cell.* 114:75–86. http://dx.doi.org/10.1016/S0092-8674(03)00477-X

Südhof, T.C., and J.E. Rothman. 2009. Membrane fusion: grappling with SNARE and SM proteins. *Science.* 323:474–477. http://dx.doi.org/10.1126/science.1161748

Suh, Y.H., A. Terashima, R.S. Petralia, R.J. Wenthold, J.T.R. Isaac, K.W. Roche, and P.A. Roche. 2010. A neuronal role for SNAP-23 in postsynaptic glutamate receptor trafficking. *Nat. Neurosci.* 13:338–343. http://dx.doi.org/10.1038/nn.2488

Suh, Y.H., A. Yoshimoto-Furusawa, K.A. Weih, L. Tessarollo, K.W. Roche, S. Mackem, and P.A. Roche. 2011. Deletion of SNAP-23 results in pre-implantation embryonic lethality in mice. *PLoS One.* 6:e18444. http://dx.doi.org/10.1371/journal.pone.0018444

Sutton, R.B., D. Fasshauer, R. Jahn, and A.T. Brunger. 1998. Crystal structure of a SNARE complex involved in synaptic exocytosis at 2.4 A resolution. *Nature.* 395:347–353. http://dx.doi.org/10.1038/26412

Tadokoro, S., N. Hirashima, and N. Utsunomiya-Tate. 2016. Effect of Complexin II on membrane fusion between liposomes containing mast cell SNARE proteins. *Biol. Pharm. Bull.* 39:446–449. http://dx.doi.org/10.1248/bpb.b15-00751

Takahashi, N., T. Kishimoto, T. Nemoto, T. Kadowaki, and H. Kasai. 2002. Fusion pore dynamics and insulin granule exocytosis in the pancreatic islet. *Science.* 297:1349–1352. http://dx.doi.org/10.1126/science.1073806

Takahashi, N., H. Hatakeyama, H. Okado, J. Noguchi, M. Ohno, and H. Kasai. 2010. SNARE conformational changes that prepare vesicles for exocytosis. *Cell Metab.* 12:19–29. http://dx.doi.org/10.1016/j.cmet.2010.05.013

Takahashi, N., W. Sawada, J. Noguchi, S. Watanabe, H. Ucar, A. Hayashi-Takagi, S. Yagishita, M. Ohno, H. Tokumaru, and H. Kasai. 2015. Two-photon fluorescence lifetime imaging of primed SNARE complexes in presynaptic terminals and β cells. *Nat. Commun.* 6:8531. http://dx.doi.org/10.1038/ncomms9531

Thorn, P., and H. Gaisano. 2012. Molecular control of compound exocytosis: A key role for VAMP8. *Commun. Integr. Biol.* 5:61–63. http://dx.doi.org/10.4161/cib.18058

Vites, O., E.L. Florin, and R. Jahn. 2008. Docking of liposomes to planar surfaces mediated by trans-SNARE complexes. *Biophys. J.* 95:1295–1302. http://dx.doi.org/10.1529/biophysj.108.129510

Wang, C.C., C.P. Ng, L. Lu, V. Atlashkin, W. Zhang, L.-F. Seet, and W. Hong. 2004. A role of VAMP8/endobrevin in regulated exocytosis of pancreatic acinar cells. *Dev. Cell.* 7:359–371. http://dx.doi.org/10.1016/j.devcel.2004.08.002

Wang, C.C., H. Shi, K. Guo, C.P. Ng, J. Li, B.Q. Gan, H. Chien Liew, J. Leinonen, H. Rajaniemi, Z.H. Zhou, et al. 2007. VAMP8/endobrevin as a general vesicular SNARE for regulated exocytosis of the exocrine system. *Mol. Biol. Cell.* 18:1056–1063. http://dx.doi.org/10.1091/mbc.E06-10-0974

Wang, G., J.W. Witkin, G. Hao, V.A. Bankaitis, P.E. Scherer, and G. Baldini. 1997. Syndet is a novel SNAP-25 related protein expressed in many tissues. *J. Cell Sci.* 110:505–513.

Washbourne, P., P.M. Thompson, M. Carta, E.T. Costa, J.R. Mathews, G. Lopez-Benditó, Z. Molnár, M.W. Becher, C.F. Valenzuela, L.D. Partridge, and M.C. Wilson. 2002. Genetic ablation of the t-SNARE SNAP-25 distinguishes mechanisms of neuroexocytosis. *Nat. Neurosci.* 5:19–26.

Weng, N., D.D.H. Thomas, and G.E. Groblewski. 2007. Pancreatic acinar cells express vesicle-associated membrane protein 2- and 8-specific populations of zymogen granules with distinct and overlapping roles in secretion. *J. Biol. Chem.* 282:9635–9645. http://dx.doi.org/10.1074/jbc.M611108200

Xie, L., D. Zhu, S. Dolai, T. Liang, T. Qin, Y. Kang, H. Xie, Y.C. Huang, and H.Y. Gaisano. 2015. Syntaxin-4 mediates exocytosis of pre-docked and newcomer insulin granules underlying biphasic glucose-stimulated insulin secretion in human pancreatic beta cells. *Diabetologia.* 58:1250–1259. http://dx.doi.org/10.1007/s00125-015-3545-4

Xu, H., M.G. Arnold, and S.V. Kumar. 2015. Differential effects of Munc18s on multiple degranulation-relevant trans-SNARE complexes. *PLoS One.* 10:e0138683. http://dx.doi.org/10.1371/journal.pone.0138683

Zheng, B., M. Sage, E.A. Sheppeard, V. Jurecic, and A. Bradley. 2000. Engineering mouse chromosomes with Cre-loxP: range, efficiency, and somatic applications. *Mol. Cell. Biol.* 20:648–655. http://dx.doi.org/10.1128/MCB.20.2.648-655.2000

Zimmermann, T.J., M. Bürger, E. Tashiro, Y. Kondoh, N.E. Martinez, K. Görmer, S. Rosin-Steiner, T. Shimizu, S. Ozaki, K. Mikoshiba, et al. 2013. Boron-based inhibitors of acyl protein thioesterases 1 and 2. *ChemBioChem.* 14:115–122. http://dx.doi.org/10.1002/cbic.201200571